applied sciences

MDPI

Review

Review of Radiation-Induced Effects in Polyimide

Elena A. Plis [1,*], Daniel P. Engelhart [1], Russell Cooper [2], W. Robert Johnston [2], Dale Ferguson [2] and Ryan Hoffmann [2]

[1] Assurance Technology Corporation, Carlisle, MA 01741, USA; engelhart@assurtech.com
[2] Air Force Research Laboratory, Space Vehicles Directorate, Kirtland AFB, Albuquerque, NM 87117, USA; russell.cooper@aero.org (R.C.); afrl.rvborgmailbox@us.af.mil (W.R.J.); afrl.rvborgmailbox@us.af.mil (D.F.); afrl.rvborgmailbox@us.af.mil (R.H.)
* Correspondence: plis@assurtech.com; Tel.: +1-505-220-3684

Received: 30 January 2019; Accepted: 5 May 2019; Published: 16 May 2019

Abstract: Polyimide (PI, Kapton-H®) films are widely utilized in the spacecraft industry for their insulating properties, mechanical durability, light weight, and chemical resistance to radiation. Still PI materials remain exposed to a combination of high-energy electrons, protons, and ultraviolet (UV) photons, particles primarily responsible for radiation-induced damage in geosynchronous Earth orbit (GEO), which drastically change PI's properties. This work reviews the effect of electron, proton, and UV photon irradiation on the material properties (morphology, absorption, mechanical properties, and charge transport) of PI. The different damaging mechanisms and chemical consequences that drive changes in the material properties of PI caused by each individual kind of irradiation will be discussed in detail.

Keywords: polyimide; geosynchronous Earth orbit (GEO); electron-irradiation; proton-irradiation; UV photons impingement; optical properties; charge transport; space weather

1. Introduction

Man-made satellites are made from many different materials; among them polyimide (PI, Kapton-H®), a solid organic insulator with a monomeric unit of $C_{22}H_{10}N_2O_5$ [1], has taken an honored place over more than four decades due to its insulating properties, mechanical durability, low density, and resistance to space radiation. PI mainly serves as the exterior surface of a satellite, offering an ultra-lightweight thermal insulator to provide a stable range of operating temperatures for satellite systems, as well as shielding electrical and electronic componentry from the space environment through which the spacecraft travels [2–5].

This paper will review the effect of the various components of the space environment, mainly geosynchronous Earth orbit (GEO), on PI's chemical structure, as well as several material properties since these changes can have profound effects on the performance of the spacecraft. The natural GEO environment comprises electrons and protons with a broad spectrum of particle energies [6–8] as well as solar ultraviolet (UV) radiation [9]. Other particles are present in GEO including gamma rays, etc., but in terms of total energy deposition into a spacecraft, solar charged particles and UV photons are the dominant species interacting with the spacecraft surface [10].

Highly energetic electrons (0.1–10 MeV) form two toroidal belts extending out to about 60,000 km (10 Earth radii, or R_E) from the Earth's center, with a maximum intensity typically at about 3–5 R_E at the equator. Thus, although GEO orbit (6.6 R_E) is beyond the distance of maximum intensity, it is well within the limits of the outer belt, and satellites orbiting within it are subjected to significant penetrating electron and proton fluxes, as can be seen in Figure 1. Solar UV radiation is often divided into two regions, the near-UV region including photon energies from 6.2–3.1 eV (200–400 nm) and vacuum-UV

(VUV) region corresponding to UV photons with wavelengths below 200 nm. The hydrogen Lyman-α line at 121.6 nm is the strongest vacuum ultraviolet (VUV) emission line in the solar spectrum [11].

When a solid dielectric interacts with energetic particles at GEO, it is subject to a number of different destructive and non-destructive processes. Non-destructive processes can result in electronic and vibrational excitation, electron emission, radiation induced conductivity, and a host of other effects that can alter spacecraft material behavior over a wide range of time scales, e.g., [12–14]. While a detailed understanding of these processes is vital to understanding and predicting a spacecraft's performance over its mission lifetime, they lie outside the scope of this review. This article will focus on the destructive processes that lead to chemical changes in spacecraft materials and how the material's physical properties change as a manifestation of that chemical damage.

The nature of the dominant mechanism of energy deposition depends strongly on the mass of the particle. Massive particles such as protons will impart large amounts of ballistic energy over a relatively short depth, displacing nuclei in the solid, exciting phonons and vibrational transitions sufficient to rupture every chemical bond [15]. Less massive particles, such as electrons, can be expected to deposit energy primarily in the form of electronic excitation. Sufficient electronic energy deposition will also rupture bonds, but the damage will be deposited over a longer trajectory and the chemical damage will be more bond-selective. UV photons are energetic enough to dissociate molecular bonds, resulting in photo-oxidation reactions that scissor or crosslink the polymer chains [16]. Indeed, even very low energy ions and low mass particles such as He^+ ions impart enough energy to break all bonds along a penetration track in principle, but experimental studies have shown that low energy and low mass particles impart damage through distinct and relatively well defined reactions [17].

Electrons, protons, and photons incident on a surface can also cause secondary electrons to be ejected, initiating a charge imbalance near the surface. The secondary electron emission probability is strongly dependent on the incident energy of the impinging particle [18–20]. Additionally, after the kinetic energy of a charged particle has been exhausted, the proton or electron can embed itself into the bulk, creating a local charge imbalance at the penetration depth of the particle. When considering the interaction of the space environment with solid dielectrics, it is important to distinguish between energy deposition and charge deposition [21]. If the charge in a material builds to a sufficient level, this can lead to a dielectric breakdown or discharge to an adjacent (lesser charged) material. Both of these electrostatic discharges can cause extensive local material damage.

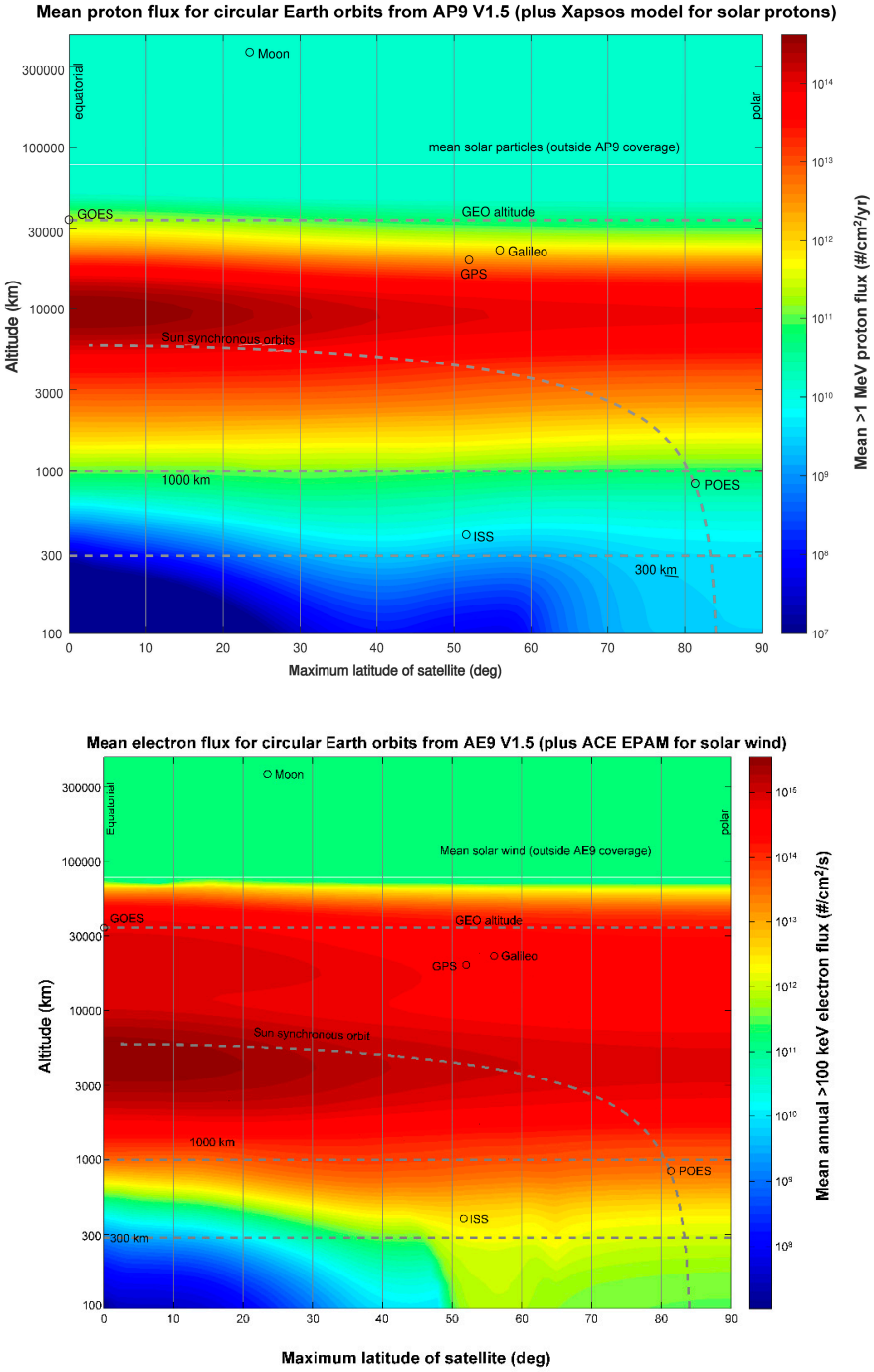

Figure 1. (Top panel) Mean annual electron flux (>100 keV electrons) and (bottom panel) mean annual proton flux (>5 MeV protons), orbit averaged, experienced by a satellite in a circular geocentric orbit as a function of altitude and maximum latitude (inclination for prograde orbits, supplement of inclination for retrograde orbits). Representative orbits are shown as dashed lines for reference, as are the positions of the Moon, International Space Station (ISS), and several other satellites. Figure based on AE9 V1.5 mean radiation belt model [22] for trapped electrons and protons, ACE EPAM data [22,23] for untrapped solar wind electrons, and the Xapsos model [24] for untrapped protons, with approximate geomagnetic cutoffs in solar proton access based on [25].

Kapton has been utilized for the spacecraft industry starting in the 1970s, and several attempts to summarize changes in its material properties, among those of other dielectrics, after interaction with charged particles have been already made [26–28]. While comprehensive, these reviews

primarily emphasize the usage of dielectrics as electrical materials, with little attention given to the changes of mechanical and optical properties and the underlying changes in the chemical structure of irradiated materials.

The radiation-induced changes to PI's material properties are the result of radiation induced effects on the material's chemical structure. Thus, for instance, increased dark conductivity of electron-irradiated PI is attributed to the presence of radicals formed as a result of radiation-induced breakage of imide rings and/or ether bridges forming a metastable carbonyl. Increased concentration of radicals, which can act as localization sites for both electrons and holes, together with increased probability of charge release rate in radiation-damaged material leads to faster movement of the charge body thus improving the conductivity of the material [29]. Since radiation induced conductivity (RIC) in PI is controlled by several competing physical processes, it is therefore dependent upon radiation dose rate, total received radiation dose, electric field, and temperature; thus, decrease and increase of RIC depending on PI's irradiation conditions has been reported [30].

The intensity of the VUV radiation is negligible (0.11 W/m^2) compared to the total electromagnetic intensity of solar radiation (1356 W/m^2). However, the effects of VUV radiation should not be neglected since complete absorption of high-energy photons in spacecraft materials can induce photolysis with subsequent formation of highly chemically reactive moieties [31]. The creation of these reactive chemical structures may result in a large variety of processes from the modification of the polymer surface to complete decomposition [32,33].

One of the critical components missing from reports of ground-based simulation of material degradation is detailed description of the sample handling procedures. It has been shown that materials damaged by charged particles or light are susceptible to quick and dramatic "healing" in the presence of air. This makes comparisons between experiments from different facilities extremely difficult and has created uncertainty in the primary driving mechanism for material damage in space as each facility's space degradation simulation has different strengths and weaknesses in simulating the space environment. In this review we will look at results regardless of the how the samples were handled, but where possible post-irradiation sample handling will be reported and a higher priority will be given to results using samples that were handled in vacuum or inert environments.

Whereas simulated spacecraft material degradation typically takes place under high vacuum conditions, ~10^{-6}–10^{-7} Torr, the subsequent material characterization is often performed in an uncontrolled laboratory atmosphere. Chemical reaction of atmospheric gases with the highly reactive radiation-modified PI may change the properties of damaged material in a way that is unrepresentative of the space environment. Throughout recent decades, limited attention has been given to the effects that the characterization/handling atmosphere has on the material properties of PI films irradiated with high energy particles. Investigators at the U.S. Air Force Research Laboratory Space Vehicles Directorate have evaluated the effects of several major constituents of Earth's atmosphere (Ar, N_2, O_2, and H_2O) on the charge transport properties of PI damaged by exposure to 90 keV electrons and found that exposure to O_2 and H_2O can have rapid and profound effects on the charge transport properties of electron irradiated PI [34]. Whereas a detailed discussion of this topic is out of scope of the presented review, we would like to emphasize the importance of careful control of the storage, handling, and characterization protocols of irradiated material.

In the present work we review the published literature on alterations of material properties of Kapton irradiated with high energy particles (electrons and protons) and VUV photons spanning the 1970s-present time period. It should be noted that vast majority of the publications reviewed here investigate the effect of applied radiation doses on the order of several MGy, corresponding to the several decades of mission duration. The typical operational lifetime of a GEO satellite currently spans between 12 and 15 years. However, these limits are usually imposed by the amount of fuel available for station-keeping [35], and the spacecraft design community strives continuously to extend the lifetime of new satellites in orbit in order to reduce launch and operation expenses [36–39], to name just a few. Thus, the operational life of GEO satellites may increase significantly in the near future

and the understanding of the PI's material changes at higher irradiation doses is important for the development of more reliable predictive spacecraft models.

Moreover, decommissioned spacecraft do not disappear from GEO; rather, they are sent to a "graveyard orbit" where they continue to age. An understanding of space-weather-induced material changes in PI at higher irradiation doses is essential in order to assist with cataloguing of the unknown objects in the GEO ring for collision risk mitigation of currently operational GEO satellites with the decommissioned GEO satellites. Additionally, space debris, especially high area to mass ratio (HAMR) objects, populate all orbits of interest and knowledge of how their optical and chemical signatures change on orbit could be useful in their characterization.

This review may be useful for the development of more reliable predictive spacecraft models (electrical charging, thermal, etc.) to guide the design of satellites with improved lifetime and system reliability, and decreased satellite operational and construction costs.

2. GEO-Environment Simulation Facilities

At GEO, space weather may be represented by a combination of high vacuum, electron (10 keV–2 MeV) and proton (10^{-4}–10 MeV) fluxes, solar photons, and thermo-cycling between 120–150 K and 400–420 K [40,41]. Several irradiation facilities are available worldwide to perform material investigations under radiation conditions that are prevalent in the space environment.

In some of them multiple radiation sources are combined in one vacuum irradiation chamber e.g., bombardment of materials with electrons and protons having energies up to 100 keV in the complex irradiation facility (CIF) at the DLR-Institute of Space Systems in Bremen, Germany [42], 116.5 nm and 123.6 nm VUV photon and up to 100 keV electron sources at the US Air Force Research Laboratory, Kirtland Air Force Base, USA [43], or 20–100 keV electrons, 30–150 keV protons, 120–1500 nm VUV photons, and 5 eV atomic oxygen sources at the Arnold Engineering Development Center (AEDC) [44]. Others allow the testing of combined effects in one location but not necessarily in the same chamber, as sets of UV, VUV, proton, and electron sources at the Boeing space and defense systems irradiation facility [45].

Most of the irradiation facilities utilize only the dominant source of energy deposition, e.g., the SIRENE facility at Toulouse, France uses 20–400 keV electron "spectrum" generated by a Van de Graff accelerator (monoenergetic, 100–400 keV) and an electron gun (monoenergetic, 1–35 keV). The monoenergetic electron beams can be attenuated using a set of diffusion windows to simulate the spectrum of electron energies found in the space environment [46]. The electron beam irradiation facility (JAEA) at Takasaki, Japan [47] uses a 1–2 MeV monoenergetic electron beam; the National Centre for Accelerator based Research (NCAR), Bilaspur, India utilizes proton and neutron sources with a wide particle energy range [48], and the Taiwan Daheng Irradiation Plant, Taiwan, Republic of China uses an electron beam for the irradiation of industrial materials [49]. A comprehensive online database of irradiation facilities around the world has been prepared by the European Organization for Nuclear Research (CERN) [50].

3. Results

3.1. Changes in Electrical Properties

The electrical properties that are of major importance to the operation and lifetime of a GEO satellite include the surface and volume resistivities of its surface materials. Figure 2 presents a plot of the surface potential decay rate as a function of dark (volume) resistivity [51]. When the charge decay time of the surface materials exceeds the orbital period (one day for GEO), the material can differentially charge throughout the entire mission and the likelihood of discharge increases. The red star in Figure 2 shows the resistivity of pristine polyimide. As shown in Figure 3, the conductivity of polyimide can increase by orders of magnitude after electron irradiation. The irradiated material can become far less susceptible to charge accumulation. Thus, an understanding of the charge conduction and dissipation mechanisms is important for the satellite designers to understand the behavior of a satellite throughout its operational lifetime.

It should be noted that the method of conductivity measurement of inhomogeneous insulators is important and depends on the application. The measurement method must be chosen carefully in order to avoid misleading results [52,53]. In order to measure the most conductive pathway through a disordered insulator, for applications such as shielding high voltage wires or microprinting electronics, where possible current leakage is the relevant property, then the ASTM standard [54] produces the relevant resistivity value. However, for spacecraft charging applications in which understanding residual surface charge due to charged particle implantation is the goal, the result given by the surface-potential decay (SPD) method is more appropriate as this will measure the least conductive domains in the inhomogeneous material [55].

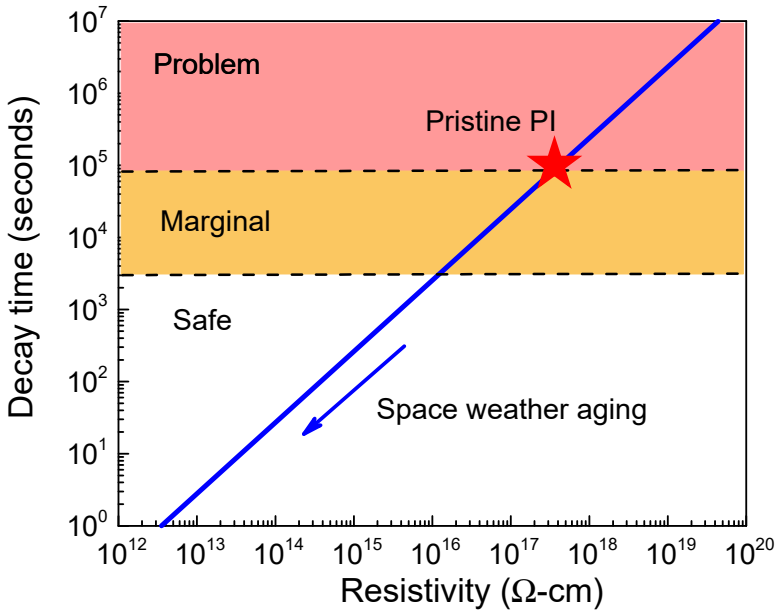

Figure 2. Plot of charge decay time versus resistivity value for PI. The red star indicates the resistivity of pristine PI. Note, that after electron irradiation the resistivity can decrease by several orders of magnitude. Adapted with modifications from [56].

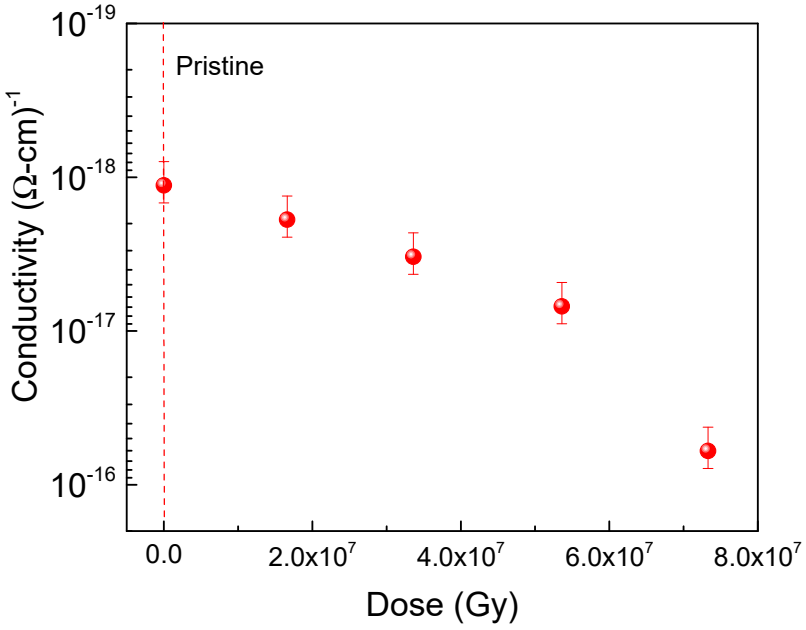

Figure 3. Conductivity of PI material irradiated with different doses.

The evolution of surface potential during electron irradiation (charge build-up) and after charging (potential decay) [55,57,58] and pulsed electro-acoustic (PEA) [59–62] measurements are considered the most significant laboratory methodologies used to investigate the PI's charging and discharging behavior in a space environment. Several different factors need to be taken into account for the development of reliable theoretical models of charge distribution and dissipation in electron-irradiated material. For example, charging involves simultaneous charge transport and electron scattering mechanisms, whereas potential decay is an even more complex process superimposing electronic excitation assisted charge transport, termed radiation induced conductivity (RIC) [63], charge capture and release by radiation-induced deep and shallow traps, surface conduction, and, possibly, polarization effects [64].

Charge build-up in electron-irradiated PI films has been extensively studied by Sessler et al. [65,66] and Cao et al. [67–69]. Excellent reviews of mechanisms accounting for the potential decay in electron-irradiated PI as well as various charge carriers transport models developed over the past several decades have been recently published by Molinie [70] and Tyutnev [71]. The various approaches for the potential build up and decay differ significantly with respect to the underlying assumptions concerning charge trap distribution, carrier mobility, charge injection methods, etc. [72,73].

A number of physical parameters related to charge carrier transport may be extracted from the fitting of experimental surface potential build up/decay curves. These parameters include, but are not limited to, the density of charge trap states, charge capture cross-section, the charge trap release and re-trap probabilities, and dark resistivity of the irradiated material. The presented paper is not intended to provide comparison between physical parameters extracted from the theoretical simulations of build-up and pre-transit regions of the surface potential versus decay time curve. Instead, attention is focused on the changes in bulk resistivity, or its inverse, conductivity, of the irradiated material.

The irradiation-induced enhancement of conductivity in polymers has been observed by numerous different research groups (e.g., [74–77]). Figure 3 presents conductivity of 76 μm PI material mounted on rotating aluminum carousel irradiated with 90 keV electrons (maximum penetration depth 83 μm) [6] versus energetic radiation dose measured under vacuum (pressure $<1 \times 10^{-6}$ Torr) with the SPD method [55]. Irradiation was performed at an accelerated dose rate of 94.8 Gy/s. The average electron flux received by PI film during irradiation was 7.8 nA/cm^2. Each SPD measurement was performed using irradiation with 5 keV electrons. During charging, a flux of ~20 nA/cm^2 was applied for less than 10 s to a fully discharged sample which had been under vacuum for a minimum of 24 hours. The initial applied surface potential was 2.5–3 kV for all tests. The dark conductivity values were derived from the slope of the SPD curve after it became linear on a log/linear plot. This regime of the SPD curve represents the regime in which the front of the charge body has already reached the grounded backing plane and the decay of surface potential may be modeled as a leaky capacitor [78].

The conductivity of electron-irradiated polyimide showed an increase of two orders of magnitude after irradiation with an initial dose of 20 MGy and further increases for larger doses, as shown in Figure 3. Similar results have been reported by other research groups [29,79,80].

The interpretation of the physical processes that cause an increase of conductivity in irradiated PI is still questionable. Generally, charge transport in disordered materials like PI occurs via incoherent electron hopping among transport sites. Bulk conductivity is influenced by both energetic and geometric disorder of electron trap sites. That is to say, the facility with which an electron can travel through a disordered material in the presence of a strong electric field is dependent on both the energetic distribution of transport sites within the material and the geometric distribution of the transport sites. The latter dependency arises due to the variation of intersite electronic wavefunction overlap originating from the positional and orientational distribution of these hopping sites [81]. Authors of the present manuscript attribute the observed dose-dependent bulk conductivity increase in irradiated PI to the radiation-induced formation of electron hopping sites and the formation of extended pi-bonded chemical structures which are not present in the pristine material. These sites are created as a result of bond-specific rupture during electron bombardment. This phenomenon is considered to be distinct

from RIC which is temporary and is the result of increased energy in the system and therefore the excitation of electrons to excited states, forming electron-hole pairs that facilitate electron mobility. This must not be confused with the creation and destruction of transport sites within the material as discussed here.

Other researchers attribute observed long-term conductivity increases after irradiation to the delayed RIC (DRIC) induced by aging [78,82–85]. At lower irradiation doses, trapped charge carriers are easily de-trapped in the conduction and valence bands, therefore a high conductivity is maintained for a long period of time without any degradation. At higher doses (>10^6 Gy), the structural damage in PI prevails over the ionization one thus causing the recovery of the conductivity values to the level of the pristine material.

There are not many studies addressing the change of PI volume charge transport characteristics after proton and VUV irradiation. Yue et al. [86,87] reported a decrease in RIC of up to three orders of magnitude for PI material irradiated with 60–110 keV protons to a maximum fluence of 10^{14} protons/cm^2, that was attributed to the pyromellitimide groups' (C-N, C=O) degradation. Further, formation of a graphite-like layer on the surface of PI samples that have been proton-irradiated with particle beams of energy ranging from 10 keV to a few MeV up to a maximum fluence of 2.4×10^{16} protons/cm^2 has been reported to cause a decrease in surface resistivity [88].

Several research groups have studied the ultraviolet-laser induced conductivity of PI films under ultraviolet laser irradiation [89–91]. A permanent increase of PI's electrical conductivity up to fifteen orders of magnitude was observed, which is attributed to the radiation-induced creation of surface conductive region. In this region, the chain scission between imide nitrogen atoms and phenyl rings of the ether segments is taking place under laser irradiation, followed by the formation of the network of fused aromatic rings with an effective π-orbital overlap facilitating the electrical conduction.

3.2. Changes in Chemical Properties

Fourier-transform infrared (FTIR) spectroscopy is a widely used and convenient tool for the characterization of chemical changes in irradiated PI. It probes chemical bonding by optically exciting vibrational transitions within the polymer. Changes in the position and intensity of the IR absorption "fingerprint" of damaged material will offer insights into what chemical bonds are being modified during the radiation-induced degradation. PI has a complex IR signature with each peak corresponding to a specific vibrational mode of one bond within the monomer; some of these characteristic vibrational assignments are summarized in Table 1 [92–98].

The formation of new absorption features has not been reported for PI material irradiated with low (5 keV)–or high (90 keV)–energy electrons. Instead, several interesting radiation-induced changes in the IR fingerprint of the damaged film were observed for the PI irradiated with 90 keV. First, the absorption at the wavelength associated with the carbonyl out-of-phase stretch (1679 cm^{-1}) increased after electron bombardment. This suggests first that existing carbonyl moieties were not preferentially broken due to electron bombardment. A concurrent reduction in the absorption associated with the ether C-O-C stretch after electron bombardment suggests that ether breakage may result in new carbonyl-like moieties. Further, peak intensity at 1780 and 1376 cm^{-1} increases after irradiation, which is generally attributed to the formation of imide rings, possibly leading to the formation of new π-bonded carbon structures [56].

Table 1. Vibrational assignments of polyimide.

Assignment (cm^{-1})	Irradiation Absorption (cm^{-1})	Characterization
568	δ(phenyl)	Phenyl ring deformation
607	δ(phenyl)	Phenyl ring deformation
636	δ(C=O)	Carbonyl deformation
705	δ(C-N-C)	Imide deformation
717	C=O	Carbonyl bending
725	δ(C-N-C)	Out-of-phase bending of imide ring
734	C=O	Carbonyl bending
752–960	δ(phenyl)	Phenyl ring deformation
1079	C-O-C stretch	Stretching deformation
1095	ν(C-N-C)	Imide stretch
1117	ν(C-N-C)	Imide stretch
1160	C-C	C-C bending
1168	ν(C-N-C)	Imide stretch
1188	δ(phenyl)	Phenyl ring deformation
1230	C-N	C-N stretch
1243	ν(C-O-C)	Bridging C-O-C stretch
1260	ν(C-O-C)	Bridging C-O-C stretch
1290–1307	δ(phenyl)	Phenyl ring deformation
1350	C-N	C-N stretch
1376	δ(C-N-C)	Imide stretch
1390	C-N	C-N stretch
1456–1600	ν(phenyl)	Phenyl ring C-C stretch
1679–1779	ν(C=O)	Carbonyl stretch
1825	Cyclic anhydrides, presented in not fully cured polymer (precurser)	
3020–3155	ν(C-H)	Phenyl ring C-H stretch
3488	ν(C-H)	Phenyl ring C-H stretch

PI irradiated with 5 keV electrons demonstrated evidence of swelling due to irradiation-induced cross-link formation [99] manifesting itself as a re-positioning of imide deformation bands in the FTIR spectrum of irradiated PI [71].

Electron paramagnetic resonance (EPR) is another tool to probe the nature of chemical changes in irradiatied material by quantification of the radiation-induced unpaired electron concentration [65,100]. The EPR spectra of PI irradiated with 90 keV electrons to the dose of 56 MGy reveals formation of ketone (predominant), phenyl and phenoxy radicals originating from the rupture and subsequent rearrangement of the imidic rings and homolytic bond scission of ether bridges, respectively.

Carbon-13 nuclear magnetic resonance (^{13}C NMR) spectra of irradiated and pristine PI revealed no qualitative differences such as removal or addition of peaks initiated by irradiation [101,102]. The nearly identical chemical shifts of the carbon resonances for irradiated and pristine samples imply that there is no effect of electron irradiation in the main chemical structure of the PI film for the electron doses investigated. The stability of the structure is believed to be due to the absence of aliphatic hydrogen in Kapton which facilitates the recombination of phenyl radicals and self- mending of irradiated Kapton [103]. The absence of new peaks can also be a result of the low relative population of ^{13}C to ^{12}C. Because the relative abundance of ^{13}C to ^{12}C is ~1%, a significant portion of the bonds in the material would have to be modified before a new peak would be apparent in the NMR spectrum.

FTIR spectra of aluminized PI film irradiated with 90 keV protons and maximum fluence of 1.0×10^{16} protons/cm^2 did not demonstrate new features; however, decreased intensity and widening of vibrational bands associated with C-C stretching of phenyl ring (1515 cm^{-1}), imide =C-N stretching (1390 cm^{-1}), and asymmetric stretching of aromatic ether C-O-C (1260 cm^{-1}) was reported [104].

Raman spectra of PI irradiated with 25 keV protons with fluence of 2.25×10^{17} protons/cm^2 demonstrated two new broad peaks at 1350 cm^{-1} and 1583 cm^{-1}, which are assigned to the D and G broad bands of disordered and ordered graphitic materials [105], respectively, along with disappearance of characteristic peaks corresponding to the C-N (1376 cm^{-1}), C=O (1780 cm^{-1}), and C=C (1613 cm^{-1})

bands [106]. This suggests that complex chemical reactions are taking place during proton irradiation of PI, including the bond breakage of the carbonyl (C=O), aromatic ether (C-O-C) moieties and a ring opening reaction of cyclic imide (C-N) accompanied, presumably, by evolution of CO into the gas phase. As a result, the surface concentration of C increases and the PI surface is transformed into a carbon-enriched structure, as confirmed by X-ray photoelectron spectroscopy (XPS) measurements of proton-irradiated PI [87]. Furthermore, the EPR measurements of PI irradiated with 100 keV–200 MeV protons with fluences of 4.0×10^{15} protons/cm^2–10^{19} protons/cm^2 [107–109] revealed the formation of long-lifetime pyrolitic carbon radicals. It should be noted that lower proton energy leads to a faster increase in the pyrolytic carbon-radical-specific population with proton fluence [110,111]. This effect can be attributed to the dependence on the rate of energy deposition with particle velocity.

Exposure of PI to UV irradiation results in the formation of a high concentration of radicals as confirmed by EPR studies [112–115]. These radicals originate from a broken C-N bond in the imide group and the C-O bond of the ether of PI [116]. Results of spectroscopic ellipsometry of UV-exposed PI films suggested that the UV generated radicals are situated near the surface of the film, with ~500 nm depth of damaged layer [117].

3.3. Change in Dielectric Properties

As reported by Alegaonkar et al. [118], the dielectric constant and dielectric loss of PI exibit changes under electron irradiation. Irradiation with 1 MeV electrons to a maximum fluence of ~10^{15} electrons/cm^2 resulted in a decrease of dielectric constant from 3.1 to 2.4, with increasing electron fluence. This is explained by the irradiaton-induced reduction of PI's density and formation of π-electron clouds with their polarization aligned in the direction of the molecular chains. The dielectric loss, ε'', increases with increasing electron fluence, as is typical for most polymer dielectrics [119]. This is attributed to the increased concentration of charged carriers and available hopping sites.

The dielectric strength of PI irradiated with 21–800 MeV protons up to a maximum fluence of 2.0×10^{16} protons/cm^2 was studied by Seidl et al. [120]. Insignificant degradation, within 90% of the value of pristine PI, was observed for the proton-irradiated material. A factor of ~2 change in dielectric loss and dielectric constant over a wide range of frequencies, attributed to irradiation-induced polymer chain scission, was reported by Shah et al. [121].

Despite chemical changes induced by VUV exposure of PI films, no significant alterations of the dielectric properties were reported. For example, a small (~8%) decrease of the index of refraction over the 300 nm–1750 nm wavelength range of the UV-exposed PI film was observed [122].

3.4. Changes in Mechanical Properties

In general, the tensile strength of a disordered polymeric material is governed by the overall tendency of the material to crosslink or undergo chain scission under exposure to radiation [123]. Depending on the type of polymer, the type of radiation, and the dose rate, either scissioning or crosslinking may dominate. It is hypothesized that high irradiation doses received by PI facilitate the overlap of zones enriched with radiation-induced highly reactive free radicals with the subsequent crosslinking of such radicals with each other [124]. Moreover, in polymers with predominant radiation-induced crosslinking the tensile strength may increase to a maximum and then decrease with increasing irradiation, suggesting that the crosslinking density may become so high that the irradiated material embrittles [125]. Computer simulation of a polyimide slab exposed to 90 keV electron beam demonstrated the significant increase of its tensile elastic modulus, suggesting the radiation-induced crosslinking in PI film. This is supported by the experimental results from both x-ray scattering and mechanical analysis [126].

Mathakari et al. [127] reported a 22%, 120%, and 199% increase in tensile strength, elongation, and Young's modulus, respectively, for PI material irradiated with a 6 MeV pulsed electron beam at a maximum fluence of 4×10^{15} electrons/cm^2. Low-energy (8 keV–40 keV) electron irradiation of the similar material at the maximum fluence of 1×10^{16} electron/cm^2 resulted in 11% and 8% decrease

in tensile strength and elongation, respectively [128–130]. Irradiation of PI films with 18–20 MeV electrons to the dose of 37 MGy at 4 K also resulted in degradation of its tensile strength [131]. Sasuga et al. [132] reported ~30% decrease in tensile strength, ~80% decrease in elongation at break, and ~8% increase in Young's modulus for PI irradiated with 2 MeV electron beam to a dose of 120 MGy.

In addition, dynamic mechanical analysis (DMA) performed on PI irradiated with 1 MeV electron beam to a dose of 15 MGy revealed the increase of loss tangent (tan σ) from 0.048 (pristine material) to 0.054 (electron-irradiated). That suggests the increase of loss modulus rather than a storage modulus, implying that irradiated PI became more viscous [133], thus supporting the hypothesis about increased chain crosslinking in irradiated PI.

The effect of irradiation of PI with 1.7 MeV electrons to a maximum dose of 5×10^6 Gy on the tribological properties of PI was studied by Pei and Wang [134]. The wear rate of the irradiated PI decreased to 5.32×10^{-6} mm^3/(N × m) compared to the 9.55×10^{-6} mm^3/(N × m) of the pristine sample. Friction tests revealed that electron irradiation did not exert much influence on the friction coefficient of PI under the experimental conditions. The changed tribological properties of PI were mainly attributed to carbonization induced by radiation, after which the wear mechanism shifted from adhesive wear and scuffing for the pristine PI to mild scuffing for the irradiated sample.

The effect of proton irradiation on the mechanical properties of PI has been investigated by several different research groups. Hill and Hopewell [135] reported reduced elongation to break (from 25% to 5%), stress to break (from 2.4×10^9 N/m^2 to 1.5 N/m^2), and fracture energy (from 7 MJ/m^2 to 1 MJ/m^2) for PI film irradiated with 3 MeV protons to the maximum dose of 75 MGy. The Young's modulus did not change significantly under the same irradiation conditions. Reduction of elongation to break after PI exposure to 45 keV–10 MeV protons with fluences of ~1.0×10^{15} protons/cm^2 was also reported by Shen et al. [128] and Kim et al. [136]. Reduced elongation at break together with increased brittleness and the hardness of proton-irradiated PI is attributed to the formation of carbon-rich moeities on the surface of the PI film as a result of bond breakage of carbonyl, ether, and cyclic imide group during proton irradiation. Formation of a surface layer enriched in carbon as a result of proton irradiation is evidenced by studies of friction and wear properties of PI irradiated with 25 keV protons with fluence of 2.25×10^{17} protons/cm^2 performed by Lv et al. [106].

VUV exposure of PI film has not been shown to significantly affect its mechanical properties. For example, the irradiation of PI film, intended to serve as a sunshield in the next generation space telescope (NGST) mission, with VUV radiation of 1000 equivalent sun hours, caused changes in the ultimate tensile strength and elongation of failure of all samples within the experimental uncertainty [137].

3.5. Changes in Physical Properties

Radiation-induced microscopic changes in the chemical state of the PI material manifest themselves as macroscopic alterations of physical properties, including color, optical transmission characteristics, and morphological changes.

3.5.1. Optical

Exposure of PI to electron or proton particles results in PI's significant darkening; PI's color changes from characteristic golden yellow of pristine PI to a dark brown color after irradiation. This is attributed to an overall increase in conjugated systems in the polymer microstructure after electron irradiation (e.g., [138], with 40 keV electrons, dose of 2.5×10^9 rads) and the formation of new chromophores and auxochromes, such as isocyano (-N=C=O), ketamine (C=C=N-), and hydroxylamine (C-O-N) groups after proton irradiation (e.g., [139], with with proton energy of 90 keV, flux of 5×10^{11} cm^{-2}s^{-1}, fluence varied in a range of 5×10^{14}–1×10^{16} cm^2). Darkening of the PI material induced by electron or proton irradiation leads to increase of solar absorption of the PI that would induce strong effects on the thermal balance of spacecraft.

Ultraviolet-visible transmission/absorption (UV-VIS) spectroscopy is widely used to access information regarding the variation in optical band-gap before and after irradiation. A red shift

of the absorption edge of irradiated PI has been reported by different research groups for different electron irradiation conditions, e.g., 3 h with 5 keV electrons [140], with 2 MeV electrons to the dose of 10 kGy [141], with 90 keV electrons to the dose of 73 MGy [142], as well as different proton irradiation experiments, e.g., with 90 keV protons with fluences of 5×10^{15} protons/cm^2–1×10^{16} protons/cm^2 [104], with 2 MeV protons with fluence of 2.6×10^{15} protons/cm^2 [143], with 170 keV protons with fluences of 2×10^{15} protons/cm^2–1×10^{16} protons/cm^2 [109], and with 0.25 MeV protons with fluence of 7.0×10^{15} protons/cm^2 [144].

Representative UV-VIS transmission spectra of pristine PI and PI irradiated with 90 keV electrons and protons are shown in Figure 4. The nearly zero transmittance at wavelengths less than ~480 nm exhibited by both pristine and damaged PI is associated with π–π* transitions in the aromatic groups [145,146].

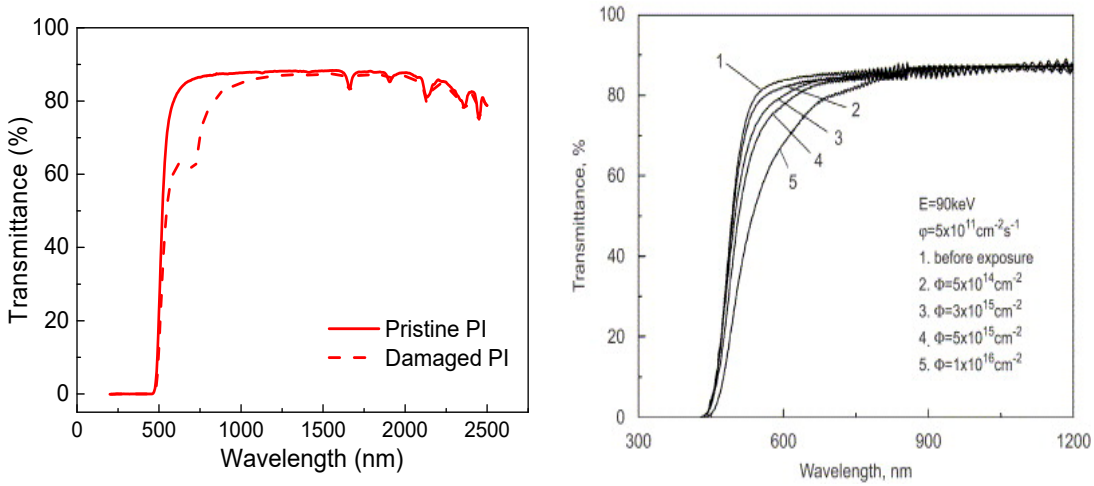

(a) (b)

Figure 4. Representative transmittance spectra of PI irradiated with (**a**) 90 keV electrons with fluence of 1.7×10^7 Gy and (**b**) 90 keV protons with different fluences. Adapted with modifications from [142] and [104], respectively.

The increased absorption in the UV/Vis spectrum of electron-irradiated PI (left panel) around 700 nm indicates an effective shrinking of the "band gap" to ~1.8 eV in the damaged material due to the presence of radiation-induced trap states. Compared to the measured "band gap" of Kapton of 2.3 eV [147], the newly created electronic states are energetically shallow. The creation of low energy electronic states coupled with the formation of radicals suggests that traps acting as new electronic transport sites are being created in the bulk. The gradual red-shift of absorption edge of proton-irradiated PI is attributed to the increasing surplus of carbon atoms formed after radiation-induced bond-breaking followed by loss of nitrogen and oxygen atoms [148,149]. A comparison of the two plots in Figure 4 shows the fundamental difference in the damage mechanism between electrons and protons.

Irradiation of PI film with VUV radiation (5–200 nm) led to a darkening of the PI material and is attributed to surface carbonification, causing significantly reduced reflectance of PI film in the 250–500 nm spectral region [137]. The VUV-induced breakage of the ether bridge oxygen and carbon-nitrogen bonds leads to the high concentration of benzene group near the surface of PI film [113].

3.5.2. Surface Morphology

Modification of the surface morphology of electron-irradiated PI may be attributed to the degassing of elements of the PI upon electron impact. However, due to the small mass of electrons, no significant roughening of surface is expected. Alegaonkar and Bhoraskar [150] noticed formation of wrinkle-like patterns on the surface of PI irradiated with 6 MeV electrons at a fluence of ~5×10^{15} electrons/cm^2.

The maximum roughness of irradiated PI exceeds that of the pristine material by a factor of six. Oppositely, Mishra et al. [151] reported that irradiation of PI with 2 MeV electrons to a dose of 26 kGy resulted in reduced mean surface roughness of irradiated material, 4.0 ± 0.5 nm, compared to the pristine PI, 5.8 ± 0.5 nm.

Due to their significantly higher mass than electrons, protons are expected to noticeably damage the exposed film resulting in its degradation. It should also be taken into account that for a given incident dose protons will do more damage to a thin film than electrons of the same energy. For instance, the maximum penetration depth of a 1 MeV proton is ~0.002 cm whereas the penetration depth for electrons of the same energy is ~0.3 cm, thus the density of deposited energy is two orders of magnitude higher for protons [6,152].

Formation of scattered blisters with size of ~10 μm on the surface of PI irradiated with 250 keV protons to the fluence of 7×10^{15} protons/cm^2 was reported by Shrinet et al. [99]. The blistering mechanism is correlated with the release and subsequent coalescence of CO molecules on the surface of PI film during proton-irradiation. A similar result was observed by Li et al. [139] for the irradiation of PI film with a 90 keV proton beam to a maximum fluence of 10^{16} protons/cm^2. RMS roughness of aluminized PI film irradiated to a fluence of 2.0×10^{15} protons/cm^2 increased by factor of ~6 due to the formation of finger-like bulges; with further irradiation these finger-like bulges were gradually stripped which reduced the RMS surface roughness.

Severe degradation of PI surface roughness with formation of humps and dents with ~20 nm height/depth, respectively, as a result of PI film exposure to the UV irradiation in a form of single UV-laser pulses with pulse durations between 140 ns and 5 μs was reported [16,153].

3.6. Other Properties

Mishra et al. [154] reported on modification of the thermal behavior of PI induced by irradiation with 2 MeV electrons to the dose of 23 kGy. The endothermic transition signifying the melting temperature of electron-irradiated PI was reduced from 387 °C in the pristine PI to 380 °C. The same research group studied the effect of 62 MeV proton irradiation on the thermal stability of PI [155]. An increase in the glass transition temperature from 280 °C in pristine PI to 290 °C for PI irradiated with a 10–60 kGy dose was observed. Changes in the thermal stability of electron- and proton-irradiated PI were attributed to the radiation-induced chain-scission and cross-linking of some of the degraded molecules by electron and proton irradiation, respectively.

The effect of electron irradiation on the free volume of PI, i.e., the volume of microvoids originating during the manufacturing process of PI, was investigated by Alegaonkar and Bhoraskar [156] and Hirade et al. [157]. The existence of large free volume in PI may affect its structural characteristics, in particular, the diffusivity of metal inclusions in irradiated PI. It was shown that electron irradiation facilitates the evolution of various gas species, such as oxygen, nitrogen, H–OH, N-H etc., from the PI matrix resulting in a decrease of the free volume. Practical applications of silver diffused PI for the realization of electron radiation resistant material were studied by Mahapatra et al. [158,159].

4. Conclusions

Understanding the effect of space weather on the electrical, mechanical, and physical properties of the commonly used spacecraft material Kapton-H® will serve to the advantage of spacecraft scientists and engineers by facilitating more efficient and robust spacecraft design. Further, detailed knowledge of how space environments interact with materials in Earth orbit will guide the development of next generation spacecraft materials.

A considerable amount of information related to the interaction of electrons, the primary damaging species in GEO in terms of energy deposition, protons, and UV photons, with Kapton-H® material is available in the literature. Whereas a representative space weather simulation would include simultaneous exposure to high energy electrons, protons, and UV photons in order to study synergistic damage processes that occur during the interaction of materials with a complicated charged particle

environment, no literature is available in open sources on the cumulative effect of GEO environment constituents on the PI film. Partially, this may be explained by the dominant role of high energy electrons in GEO environment and the experimental hurdles involved in simultaneous exposure.

It should also be noted that despite the efforts of many researchers over the past decades, understanding of damage mechanisms resulting from the electron and proton irradiation of PI film are still somewhat unclear. For example, the computer simulation of a PI slab exposed to a 90 keV electron beam suggested radiation-induced crosslinking in PI film; this conclusion was supported by the experimental results from both the x-ray scattering and mechanical analysis [126]. However, thermogravimetric analysis performed on electron-damaged PI film by Mishra et al. [154] suggests the polymer chain-scission as a dominant effect of electron irradiation. Still, work by Marletta and Iacona suggests that the mechanism of energy release and consecutive damage to the solid will be qualitatively different for protons and electrons since it depends on the mass and/or the energy of the bombarding particles [17].

Last but not least, we want to briefly discuss the industrial applications of polymers modified with ionizing radiation. An excellent review on radiation-assisted processes of various polymers and their commercial applications was recently published by Clough [160]. Generally, ionizing radiation is widely used for the development of advanced polymeric materials for a broad range of industries, including the production of insulating (e.g., [161–165]), heat-shrink (e.g., [166–168]), and shape-memory materials (e.g., [169–174]).

The development of novel engineered materials involving the exposure of PI to high energy ionizing radiation is an actively evolving engineering field where the efforts of many researchers are focused. Reports on PI irradiation with electron beams of different energy and exposure to VUV photons (usually in the form of laser irradiation) to improve PI's radiation resistance (e.g., [175]) and surface properties (e.g., [19,176–181]) have been published. Moreover, efforts were undertaken to improve the atomic oxygen (AO) erosion resistance of PI for low Earth orbit (LEO) applications. Along with the deposition of thin protective oxide or alloy coatings on PI surface (e.g., [182–191]), the incorporation of phosphorus-containing functional groups into the polyimide chemical structure attracted the researchers' attention as a viable alternative for the development of materials with improved AO erosion resistance (e.g., [192–201]). However, the detailed review of the AO erosion protection techniques for the improved PI performance at LEO as well as PI modifications with energetic species commonly found at LEO and is out of scope of the presented paper.

In conclusion, this paper presents our best effort to compile the information available over the past four decades on the alterations of material properties of PI under a simulated GEO environment as well as the underlying chemistry that drives these changes. While the information presented here may not be exhaustive, it serves to illustrate the broad variety of chemical and physical changes that can occur in a given material under space-like conditions and the importance of understanding the damage mechanisms of each species individually and cumulatively.

Author Contributions: Conceptualization, E.A.P., D.P.E., and R.H.; Writing-Original Draft Preparation, E.A.P.; Writing-Review & Editing, E.A.P., D.P.E., R.C., W.R.J., R.H.; Funding Acquisition, D.P.E. and R.H.

Funding: This research was funded by Air Force Office of Scientific Research, Remote Sensing and Imaging Physics Portfolio (Stacy Williams) grant 17RVCOR414.

Conflicts of Interest: The authors declare no conflict of interest. The funders had no role in the design of the study; in the collection, analyses, or interpretation of data; in the writing of the manuscript, and in the decision to publish the results.

References

1. Sroog, C.E.; Endrey, A.L.; Abramo, S.V.; Berr, C.E.; Edwards, W.M.; Olivier, K.L. Aromatic polypyromellitimides from aromatic polyamic acids. *J. Polym. Sci.* **1965**, *3*, 1373–1390. [CrossRef]
2. Iyer, K.A.; Mehoke, D.S.; Batra, R.C. Interplanetary Dust Particle Shielding Capability of Spacecraft Multilayer Insulation. *J. Spacecr. Rocket.* **2015**, *52*, 584–594. [CrossRef]

3. Christiansen, E.L.; Lear, D.M. Toughened Thermal Blanket for Micrometeoroid and Orbital Debris Protection. *Procedia Eng.* **2015**, *103*, 73–80. [CrossRef]
4. Mazzinghi, A.; Sabbadini, M.; Freni, A. Enhanced RF Behavior Multi-Layer Thermal Insulation. *Sci. Rep.* **2018**, *8*, 91. [CrossRef]
5. Hołyńska, M.; Tighe, A.; Semprimoschnig, C. Coatings and Thin Films for Spacecraft Thermo-Optical and Related Functional Applications. *Adv. Mater. Intterfaces* **2018**, *5*, 1701644. [CrossRef]
6. Berger, M.J.; Coursey, J.S.; Zucker, M.A.; Chang, J. *ESTAR, PSTAR, and ASTAR: Computer Programs for Calculating Stopping-Power and Range Tables for Electrons, Protons, and Helium Ions (Version 1.2.1)*; National Institute of Standards and Technology: Gaithersburg, MD, USA, 1999. Available online: http://physics.nist.gov/Star (accessed on 11 November 2018).
7. Jursa, A.S.; Laboratory USAFG. *Handbook of Geophysics and the Space Environment*; Air Force Geophysics Laboratory, Air Force Systems Command, U.S. Air Force: Baltimore, Maryland, 1985.
8. Ginet, G.; O'Brien, T.; Huston, S.; Johnston, W.; Guild, T.; Friedel, R.; Lindstrom, C.D.; Roth, C.J.; Whelan, P.; Quinn, R.A.; et al. AE9, AP9 and SPM: New models for specifying the trapped energetic particle and space plasma environment. *Space Sci. Rev.* **2013**, *179*, 579–615. [CrossRef]
9. Paillous, A. Radiation damage to surface and structure materials. In *The Behavior of Systems in the Space Environment*; Springer: Dordrecht, The Netherlands, 1993; pp. 383–405.
10. Pilipenko, V.; Yagova, N.; Romanova, N.; Allen, J. Statistical relationships between satellite anomalies at geostationary orbit and high-energy particles. *Adv. Space Res.* **2006**, *37*, 1192–1205. [CrossRef]
11. Schühle, U.; Halain, J.-P.; Meining, S.; Teriaca, L. The Lyman-alpha telescope of the extreme ultraviolet imager on solar orbiter. *Proc. SPIE* **2011**, *8148*, 81480K-1–81480K-11. [CrossRef]
12. Sato, N.; Suzuki, K.; Chiba, U.; Miyake, H.; Tanaka, Y.; Okumura, T.; Kawakita, S.; Takahashi, M.; Koga, K. Photoelectron Emission on Polyimide Films Irradiated by Proton. In Proceedings of the IEEE 2018 Condition Monitoring and Diagnosis (CMD), Perth, WA, Australia, 23–26 September 2018; pp. 1–4. [CrossRef]
13. Arnaout, M.; Paulmier, T.; Dirassen, B.; Payan, D. Study of radiation induced conductivity and photoconduction phenomenon for materials used in space environment. *J. Electrost.* **2016**, *84*, 48–53. [CrossRef]
14. Wu, J.; Miyahara, A.; Khan, A.; Iwata, M.; Toyoda, K.; Cho, M.; Zheng, X. Effects of energetic electron and proton irradiation on electron emission yield of polyimide induced by electron and photon. *Trans. Jpn. Soc. Aeronaut. Space Sci.* **2014**, *12*, 13–19. [CrossRef]
15. Marletta, G.; Iacona, F. Heat-induced versus particle-beam-induced chemistry in polyimide. *Nucl. Instrum. Methods Phys. Res. B* **1993**, *80*, 1045–1049. [CrossRef]
16. Qu, C.; Hu, J.; Liu, X.; Li, Z.; Ding, Y. Morphology and Mechanical Properties of Polyimide Films: The Effects of UV Irradiation on Microscale Surface. *Materials* **2017**, *10*, 1329. [CrossRef]
17. Marletta, G.; Iacona, F. Chemical and Physical Property Modifications Induced by Ion Irradiation in Polymers. In *Materials and Processes for Surface and Interface Engineering. NATO ASI Series (Series E: Applied Sciences)*; Pauleau, Y., Ed.; Springer: Dordrecht, The Netherlands, 1995; Volume 290. [CrossRef]
18. Dennison, J.R.; Sim, A.; Thomson, C. Evolution of the Electron Yield Curves of Insulators as a Function of Impinging Electron Fluence and Energy. *IEEE Trans. Plasma Sci.* **2006**, *34*, 2204–2218. [CrossRef]
19. Wilson, G.; Dennison, J.R. Approximation of range in materials as a function of incident electron energy. *IEEE Trans. Plasma Sci.* **2012**, *40*, 291–297. [CrossRef]
20. Dennison, J.R.; Lundgreen, P.; Christensen, J. Parameterization of Secondary and Backscattered Electron Yields for Spacecraft Charging. 2018. Available online: https://digitalcommons.usu.edu/mp_post/74 (accessed on 14 June 2018).
21. Marletta, G. Chemical reactions and physical property modifications induced by keV ion beams in polymers. *Nucl. Instrum. Methods Phys. Res. B* **1990**, *46*, 295–305. [CrossRef]
22. O'Brien, T.P.; Johnston, W.R.; Huston, S.L.; Roth, C.J.; Guild, T.B.; Su, Y.J.; Quinn, R.A. Changes in AE9/AP9-IRENE Version 1.5. *IEEE Trans. Nucl. Sci.* **2018**, *65*, 462–466. [CrossRef]
23. Space Weather Prediction Center: US National Oceanographic and Atmospheric Administration. 2018. Available online: https://www.swpc.noaa.gov/products/ace-real-time-solar-wind (accessed on 5 June 2018).
24. Xapsos, M.A.; Stauffer, C.; Gee, G.B.; Barth, J.L.; Stassinopoulos, E.G.; McGuire, R.E. Model for solar proton risk assessment. *IEEE Trans. Nucl. Sci.* **2004**, *51*, 3394–3398. [CrossRef]

25. Tyssey, H.N.; Stadsnes, J. Cutoff latitude variation during solar proton events: Causes and consequences. *J. Geophys. Res. Space Phys.* **2015**, *120*, 553–563. [CrossRef]
26. Wall, J.A.; Burke, E.A.; Frederickson, A.R. *Results of Literature Search on Dielectric Properties and Electron. Interaction Phenomena Related to Spacecraft Charging*; NASA Report; NASA: Washington, DC, USA, 1977.
27. Rose, M.F. Electrical insulation and dielectrics in the space environment. *IEEE Trans. Electr. Insul.* **1987**, *5*, 555. [CrossRef]
28. Laghari, J.R.; Hammoud, A.N. A brief survey of radiation effects on polymer dielectrics. *IEEE Trans. Nucl. Sci.* **1990**, *37*, 1076. [CrossRef]
29. Plis, E.; Engelhart, D.P.; Barton, D.; Cooper, R.; Ferguson, D.; Hoffmann, R. Degradation of polyimide under exposure to 90 keV electrons. *Phys. Status Solidi B* **2017**, *254*, 1600819. [CrossRef]
30. Paulmier, T.; Dirassen, B.; Arnaout, M.; Payan, D.; Balcon, N. Radiation-Induced Conductivity of Space Used Polymers Under High Energy Electron Irradiation. *IEEE Trans. Plasma Sci.* **2015**, *43*, 2907–2914. [CrossRef]
31. Stiegman, A.E.; Liang, R.H. Ultraviolet and vacuum-ultraviolet radiation effects on spacecraft thermal control materials. In *The Behavior of Systems in the Space Environment*; Springer: Dordrecht, The Netherlands, 1993; pp. 259–266.
32. Kan, H.K.A. Space environment effects on spacecraft surface materials. *Proc. SPIE* **1985**, *541*, 164–180. [CrossRef]
33. Lippert, T. Interaction of photons with polymers: From surface modification to ablation. *Plasma Process. Polym.* **2005**, *2*, 525–546. [CrossRef]
34. Plis, E.; Engelhart, D.P.; Cooper, R.; Ferguson, D.C.; Hoffmann, R. Effect of environment on charge transport properties of polyimide films damaged by high-energy electron radiation. *J. Vac. Sci. Technol. B* **2018**, *36*, 52906. [CrossRef]
35. Galabova, K.K.; de Weck, O.L. Economic case for the retirement of geosynchronous communication satellites via space tugs. *Acta Astronaut.* **2006**, *58*, 485–498. [CrossRef]
36. Du, X.; Liang, B.; Xu, W.; Qiu, Y. Pose measurement of large non-cooperative satellite based on collaborative cameras. *Acta Astronaut.* **2011**, *68*, 2047–2065. [CrossRef]
37. Kaiser, C.; Sjöberg, F.; Delcura, J.M.; Eilertsen, B. SMART-OLEV—An orbital life extension vehicle for servicing commercial spacecrafts in GEO. *Acta Astronaut.* **2008**, *63*, 400–410. [CrossRef]
38. Chen, X.Q.; Yu, J. Optimal mission planning of GEO on-orbit refueling in mixed strategy. *Acta Astronaut.* **2017**, *133*, 63–72. [CrossRef]
39. Han, C.; Zhang, S.; Wang, X. On-orbit servicing of geosynchronous satellites based on low-thrust transfers considering perturbations. *Acta Astronaut.* **2019**. [CrossRef]
40. Mateo-Velez, J.-C.; Sicard-Piet, A.; Lazaro, D.; Inguimbert, V.; Sarrailh, P.; Hess, S.; Maget, V.; Payan, D. Severe Geostationary Environments: Numerical Estimation of Spacecraft Surface Charging from Flight Data. *J. Spacecr. Rocket.* **2016**, *53*, 304–316. [CrossRef]
41. Iucci, N.; Levitin, A.E.; Belov, A.V.; Eroshenko, E.A.; Ptitsyna, N.G.; Villoresi, G.; Chizhenkov, G.V.; Dorman, L.I.; Gromova, L.I.; Parisi, M.; et al. Space weather conditions and spacecraft anomalies in different orbits. *Space Weather* **2005**, *3*, S01001–S01016. [CrossRef]
42. Renger, T.; Sznajder, M.; Witzke, A.; Geppert, U. The Complex Irradiation Facility at DLR-Bremen. In *Advances in Solar Sailing*; Macdonald, M., Ed.; Springer: Berlin/Heidelberg, Germany, 2014. [CrossRef]
43. Cooper, R.; Hoffmann, R. *Jumbo Space Environment Simulation and Spacecraft Charging Chamber Characterization*; Air Force Report No. AFRL-RV-PS-TP-2015-0012; Air Force Research Laboratory: Albuquerque, NM, USA, 2015.
44. Test Facility Guide. Available online: https://www.arnold.af.mil/Portals/49/documents/AFD-080625-010.pdf?ver=2016-06-16-100801-260 (accessed on 1 July 2018).
45. Boeing Radiation Effect Laboratory. Available online: http://www.boeing.com/specialty/radiation-effects-laboratory/index.page (accessed on 7 July 2018).
46. Dirassen, B.; Levy, L.; Reulet, R.; Payan, D. ; Fletcher, K. (Compiler) ESA SP-540. The SIRENE facility—An improved method for simulating the charge of dielectrics in a charging electron environment. In Proceedings of the 9th International Symposium on Materials in a Space Environment, Noordwijk, The Netherlands, 16–20 June 2003; ESA Publications Division: Noordwijk, Netherlands, 2003; pp. 351–358, ISBN 92-9092-850-6.
47. National Institutes for Quantum and Radiological Science and Technology. Available online: http://www.taka.qst.go.jp/tiara/665/english/Acc_index.php (accessed on 10 July 2018).

48. Bajpai, P.K.; Trivedi, T.; Patel, S.P.; Mallik, C.; Chaturvedi, L. National Centre for Accelerator based Research at GGV Bilaspur: Emerging facility for Neutron Generation. *Proc. Dae Symp. Nucl. Phys.* **2013**, *58*, 962–963. Available online: www.sympnp.org/proceedings (accessed on 15 July 2018).
49. Taiwan Daheng Irradiation Plant. Available online: http://www.dasheng.com/en/taiwan.html (accessed on 15 July 2018).
50. Irradiation Facilities Database. Available online: http://irradiation-facilities.web.cern.ch/ (accessed on 15 July 2018).
51. Hoffmann, R.; Dennison, J.R.; Thomson, C.D.; Albretsen, J. Low-fluence Electron Yields of Highly Insulating Materials. *IEEE Trans. Plasma Sci.* **2008**, *36*, 2238–2245. [CrossRef]
52. Frederickson, A.R.; Dennison, J.R. Measurement of conductivity and charge storage in insulators related to spacecraft charging. *IEEE Trans. Nucl. Sci.* **2003**, *50*, 2284–2291. [CrossRef]
53. Plis, E.A.; Engelhart, D.P.; Likar, J.; Hoffmann, R.C.; Cooper, R.; Ferguson, D. Electrical behavior of carbon-loaded Kapton for spacecraft applications. *J. Spacecr. Rocket.* **2017**, *55*, 775–777. [CrossRef]
54. ASTM. *Standard Test. Methods for DC Resistance or Conductance of Insulating Materials*; ASTM: West Conshohocken, PA, USA, 2015.
55. Dennison, J.R.; Brunson, J.; Swaminathan, P.; Green, N.W.; Frederickson, A.R. Methods for High Resistivity Measurements Related to Spacecraft-Charging. *IEEE Trans. Plasma Sci.* **2006**, *34*, 2191–2203. [CrossRef]
56. Engelhart, D.P.; Plis, E.A.; Cooper, R.; Ferguson, D.; Johnston, W.R.; Hoffmann, R.C. Space Plasma Interactions with Spacecraft Materials. In *Plasma Science and Technology—Basic Fundamentals and Modern Applications*; InTechOpen Limited: London, UK, 2018. [CrossRef]
57. Frederickson, A.R.; Benson, C.E.; Bockman, J.F. Measurement of charge storage and leakage in polyimides. *Nucl. Instrum. Methods Phys. Res. B* **2003**, *208*, 454–460. [CrossRef]
58. Paulmer, T.; Dirassen, B.; Payan, D.; van Eesbeek, M. Material charging in space environment: Experimental test simulation and induced conductive mechanisms. *IEEE Trans. Dielectr. Elect. Insul.* **2009**, *16*, 682–688. [CrossRef]
59. Motyl, E. Electrode effects and electrical conduction in polyimide Kapton HN films. In Proceedings of the IEEE Proceedings of 6th International Conference on Conduction and Breakdown in Solid Dielectrics, Vasteras, Sweden, 22–25 June 1998; pp. 237–240. [CrossRef]
60. Perrin, C.; Griseri, V.; Inguimbert, C.; Laurent, C. Analysis of internal charge distribution in electron irradiated polyethylene and polyimide films using a new experimental method. *J. Phys. D Appl. Phys.* **2008**, *41*, 205417. [CrossRef]
61. Tanaka, Y.; Fukuyoshi, F.; Osawa, N.; Miyake, H.; Takada, T.; Watanabe, R.; Tomita, N. Acoustic measurement techniques for bulk charge distribution in dielectrics irradiated by electron beam. In Proceedings of the IEEE Proceedings of International Conference on Solid Dielectrics, Toulouse, France, 5–9 July 2004; Volume 2, pp. 940–943. [CrossRef]
62. Mo, Y.; Zhang, L.; Zhou, Y.; Liu, J.; Zhang, Y.; Zhou, Z. Space charge characteristics of thermally and electrically aged polyimide films. In Proceedings of the 12th International Conference on the Properties and Applications of Dielectric Materials (ICPADM), Xi'an, China, 20–24 May 2018; pp. 1053–1056. [CrossRef]
63. Dennison, J.; Gillespie, J.; Hodges, J.; Hoffmann, R.; Abbott, J.; Hunt, A.W. Radiation Induced Conductivity of Highly-Insulating Spacecraft Materials. In Proceedings of the 10th Spacecraft Charging Technology Conference, Biarritz, France, 18–21 June 2007.
64. Blaise, G. Charge localization and transport in disordered dielectric materials. *J. Electrostat.* **2001**, *50*, 69–89. [CrossRef]
65. Sessler, G.M. Charge dynamics in irradiated polymers. *IEEE Trans. Electr. Insul.* **1992**, *27*, 23–42. [CrossRef]
66. Sessler, G.M.; Yang, G.M. Charge dynamics in electron-irradiated polymers. *Braz. J. Phys.* **1999**, *29*, 233–240. [CrossRef]
67. Cao, M.; Wang, F.; Liu, J.; Zhang, H.-B. Charging dynamics of a polymer due toelectron irradiation: A simultaneous scattering-transport model and preliminary results. *Chin. Phys. B* **2012**, *21*, 127901. [CrossRef]
68. Feng, G.B.; Cao, M.; Yan, L.P.; Zhang, H.B. Combined effects of sample parameters on polymer charging due to electron irradiation: A contour simulation. *Micron* **2013**, *52–53*, 62–66. [CrossRef]
69. Li, W.Q.; Zhang, H.B. The surface potential of insulating thin films negatively charged by a low-energy focused electron beam. *Micron* **2010**, *41*, 416–422. [CrossRef]
70. Molinie, P. A review of mechanisms and models accounting for surface potential decay. *IEEE Trans. Plasma Sci.* **2012**, *40*, 167–176. [CrossRef]

71. Tyutnev, A.; Saenko, V.; Pozhidaev, E.; Ikhsanov, R. Experimental and theoretical studies of radiation-induced conductivity in spacecraft polymers. *IEEE Trans. Plasma Sci.* **2015**, *43*, 2915–2924. [CrossRef]
72. Sessler, G.M. Charge distribution and transport in polymers. *IEEE Trans. Dielectr. Electr. Insul.* **1997**, *4*, 614–628. [CrossRef]
73. Liu, J.; Zhang, H.B. Analysis of microscopic parameters of surface charging in polymer caused by defocused electron beam irradiation. *Micron* **2014**, *67*, 74–80. [CrossRef]
74. Yang, G.M.; Sessler, G.M. Radiation-induced conductivity in electron-beam irradiated insulating polymer films. *IEEE Trans. Electr. Insul.* **1992**, *27*, 843–848. [CrossRef]
75. Gross, B.; Faria, R.M.; Ferreira, G.F. Radiation induced conductivity in Teflon irradiated by X-rays. *J. Appl. Phys.* **1981**, *52*, 571–578. [CrossRef]
76. Tyutnev, A.P.; Saenko, V.S.; Smirnov, I.A.; Pozhidaev, E.D. Radiation-induced conductivity in polymers during long-term irradiation. *High Energy Chem.* **2006**, *40*, 319–330. [CrossRef]
77. Hanna, R.; Paulmier, T.; Molinie, P.; Belhaj, M.; Dirassen, B.; Payan, D.; Balcon, N. Radiation induced conductivity in space dielectric materials. *J. Appl. Phys.* **2014**, *115*, 33713. [CrossRef]
78. Paulmier, T.; Dirassen, B.; Rey, R. Electrostatic behaviour of space used materials in regard of internal charging met on spacecrafts. *J. Electrostat.* **2018**, *92*, 66–74. [CrossRef]
79. Treadaway, M.J.; Mallon, C.E.; Flanagan, T.M.; Denson, R.; Wenaas, E.P. The effects of high-energy electrons on the charging of spacecraft dielectrics. *IEEE Trans. Nucl. Sci.* **1979**, *26*, 5101–5106. [CrossRef]
80. Hoffmann, R.; Cooper, R.; Ferguson, D. Changes of the Electrical and Optical Character of Polyimide Films Due to Exposure to High Energy GEO-like Electrons and the Chemistry that Drives it. In Proceedings of the Advanced Maui Optical and Space Surveillance Technologies Conference, Maui, HI, USA, 15–18 September 2014.
81. Gartstein, Y.N.; Conwell, E.M. Off-diagonal disorder and activation-energy of high-field hopping motion. *Phys. Rev. B* **1995**, *51*, 6947–6952. [CrossRef]
82. Levy, L.; Paulmier, T.; Dirassen, B.; Inguimbert, C.; van Eesbeek, M. Aging and Prompt Effects on Space Material Properties. *IEEE Trans. Plasma Sci.* **2008**, *36*, 2228–2237. [CrossRef]
83. Molinie, P.; Dessante, P.; Hanna, R.; Paulmier, T.; Dirassen, B.; Belhaj, M.; Payan, D.; Balcon, N. Polyimide and FEP charging behavior under multienergetic electron-beam irradiation. *IEEE Trans. Dielect. Electr. Insul.* **2012**, *19*, 1215–1220. [CrossRef]
84. Paulmier, T.; Hanna, R.; Belhaj, M.; Dirassen, B.; Payan, D.; Balcon, N.; Tonon, C.; Dantras, E.; Bernès, A. Aging Effect and Induced Electric Phenomena on Dielectric Materials Irradiated with High Energy Electrons. *IEEE Trans. Plasma Sci.* **2013**, *41*, 3422–3427. [CrossRef]
85. Paulmier, T.; Dirassen, B.; Payan, D.; Arnaout, M. Analysis of charge transport and ionization effect in space-used polymers under high-energy electron irradiation. *IEEE Trans. Plasma Sci.* **2017**, *45*, 1933–1937. [CrossRef]
86. Yue, L.; Wu, Y.; Sun, C.; Shi, Y.; Zhang, Y. Effects of proton pre-irradiation on radiation induced conductivity of polyimide. *Rad. Phys. Chem.* **2016**, *119*, 130–135. [CrossRef]
87. Yue, L.; Wang, X.; Wu, Y.; Cao, J.L.; Liu, Y.; Sun, C.; Yang, J. Study on evolution of deep charge traps in polyimide irradiated by low-energy protons using photo-stimulated discharge technique. *J. Phys. D Appl. Phys.* **2013**, *46*, 145502. [CrossRef]
88. Hude, V.; Robben, A.P. Investigation of the effect of proton irradiation on the insulation properties of Kapton. In Proceedings of the ESA, European Space Power Conference, Tarragona, Spain, 21–25 September 1998; Volume 2, pp. 627–631.
89. Schumann, M.; Sauerbrey, R.; Smayling, M.C. Permanent increase of the electrical conductivity of polymers induced by ultraviolet laser radiation. *Appl. Phys. Lett.* **1991**, *58*, 428–430. [CrossRef]
90. Feurer, T.; Sauerbrey, R.; Smayling, M.C.; Story, B.J. Ultraviolet-Laser-Induced Permanent Electrical Conductivity in Polyimide. *Appl. Phys. A* **1993**, *56*, 275–281. [CrossRef]
91. Srinivasan, R.; Hall, R.R.; Wilson, W.D.; Loehle, W.D.; Allbee, D.C. Ultraviolet laser irradiation of the polyimide, PMDA-ODA (Kapton™), to yield a patternable, porous, electrically conducting carbon network. *Synth. Met.* **1994**, *66*, 301–307. [CrossRef]
92. Nurmukhametov, R.; Likhachev, D.Y.; Lavrov, S.; Kardash, J.Y. Features of electronic absorption spectra of aromatic polyimides and polyisoimides. *Polym. Sci. USSR* **1989**, *31*, 434–440. [CrossRef]

93. Ortelli, E.; Geiger, F.; Lippert, T.; Wokaun, A. Pyrolysis of Kapton® in air: An in situ DRIFT study. *Appl. Spectrosc.* **2001**, *55*, 412–419. [CrossRef]
94. Steckenreiter, T.; Balanzat, E.; Fuess, H.; Trautmann, C. Pyrolytic effects induced by energetic ions in polymers. *Nucl. Instrum. Meth. B* **1999**, *151*, 161–168. [CrossRef]
95. Ha, K.; West, J.L. Studies on the photodegradation of polarized UV-exposed PMDA–ODA polyimide films. *J. Appl. Polym. Sci.* **2002**, *86*, 3072–3077. [CrossRef]
96. Engelhart, D.P.; Plis, E.; Humagain, S.; Greenbaum, S.; Ferguson, D.; Cooper, R.; Hoffmann, R. Chemical and Electrical Dynamics of Polyimide Film Damaged by Electron Radiation. *IEEE Trans. Plasma Sci.* **2017**, *45*, 2573–2577. [CrossRef]
97. Guenther, M.; Gerlach, G.; Suchaneck, G.; Sahre, K.; Eichhorn, K.-J.; Wolf, D.B.; Deineka, A.; Jastrabik, L. Ion-Beam Induced Chemical and Structural Modification in Polymers. *Surf. Coat. Technol.* **2002**, *158–159*, 108–113. [CrossRef]
98. Atta, A. Modification of the Surface Properties of Polyimide Films Using Oxygen Plasma Exposure. *Arab J. Nucl. Sci. Appl.* **2013**, *46*, 115–123.
99. Shrinet, V.; Chaturvedi, U.K.; Agrawal, S.K.; Rai, V.N.; Nigam, A.K. Effect of Neutron and Proton Irradiation on Some Properties of Kapton. In *Polyimides*; Mittal, K.L., Ed.; Springer: Boston, MA, USA, 1984. [CrossRef]
100. Humagain, S.; Jhonson, J.; Stallworth, P.; Engelhart, D.; Plis, E.; Ferguson, D.; Cooper, R.; Hoffmann, R.; Greenbaum, S. Study of Damage and Recovery of Electron Irradiated Polyimide using EPR and NMR Spectroscopy. In Proceedings of the APS Meeting, New Orleans, Louisiana, 13–17 March 2017.
101. Havens, J.R.; Ishida, H.; Koenig, J.L. 1. High-resolution carbon-13 nuclear magnetic resonance study of conjugation in solid polyimides. *Macromolecules* **1981**, *14*, 1327–1333. [CrossRef]
102. O'Donnell, J.H.; Whittaker, A.K. The high resolution 13C NMR spectrum of poly(*N*,*N*′-bis(phenoxyphenyl) pyromellitimide), (Kapton). *Polym. Bull.* **1984**, *12*, 319. [CrossRef]
103. Long, E.R., Jr.; Long, S.A.T. *Spectroscopic Comparison of Effects of Electron Radiation on Mechanical Properties of Two Polyimides*; NASA Report; NASA: Washington, DC, USA, 1987.
104. Li, R.; Li, C.; He, S.; Di, M.; Yang, D. Radiation effect of keV protons on optical properties of aluminized Kapton film. *Rad. Phys. Chem.* **2007**, *76*, 1200–1204. [CrossRef]
105. Choudhary, S.; Mungse, H.P.; Khatri, O.P. Dispersion of alkylated graphene in organic solvents and its potential for fabrication applications. *J. Mater. Chem.* **2012**, *22*, 21023–21039. [CrossRef]
106. Lv, M.; Zheng, F.; Wang, Q.; Wang, T.; Liang, Y. Effect of proton irradiation on the friction and wear properties of polyimide. *Wear* **2014**, *316*, 30–36. [CrossRef]
107. Sun, C.; Wu, Y.; Xiao, J.; Yu, S.; Yi, Z.; Shen, Z.; Wang, L.; Wang, Y. Proton flux effects and prediction on the free radicals behaviors of polyimide in vacuum using EPR measurements in ambient. *Nucl. Instr. Meth. Phys. Res. B* **2017**, *397*, 39–44. [CrossRef]
108. Edwards, D.L.; de Groh, K.K.; Nehls, M.; Miller, S.K.; Banks, B.; Stephens, C.; Artiaga, R.; Benson, R.; Balascuta, S.; Zaleski, J.M.; et al. Spectroscopic investigations on the effect of proton bombardement of polyimide. *Mater. Res. Soc. Symp. Proc.* **2005**, *851*, NN 9.6.1. [CrossRef]
109. Wu, Y.; Sun, C.; Xiao, J.; Li, R.; Yang, D.; He, S. A study on the free-radical evolution and its correlation with the optical degradation of 170 keV proton-irradiated polyimide. *Polym. Degr. Stab.* **2010**, *95*, 1219–1225. [CrossRef]
110. Sun, C.; Wu, Y.; Xiao, J.; Li, R.; Yang, D.; He, S. Pyrolytic carbon free-radical evolution and irradiation damage of polyimide under low energy proton irradiation. *J. Appl. Phys.* **2011**, *110*, 124909. [CrossRef]
111. Sun, C.; Wu, Y.; Yue, L.; Sh, Y.; Xiao, J. Investigation on the recombination kinetics of the pyrolytic free-radicals in the irradiated polyimide. *Nucl. Instr. Meth. Phys. Res. B* **2012**, *271*, 61–64. [CrossRef]
112. Hill, D.J.T.; Rasoull, F.A.; Forsythe, J.S.; O'Donnell, J.H.; Pomery, P.J.; George, G.A.; Young, P.R.; Connell, J.W. Effect of simulated low Earth orbit radiation on polyimides (UV degradation study). *J. Appl. Polym. Sci.* **1995**, *58*, 1847–1856. [CrossRef]
113. Peng, G.R.; Hao, W.; Yang, D.; He, S. Degradation of polyimide film under vacuum ultraviolet irradiation. *J. Appl. Polym. Sci.* **2004**, *94*, 1370–1374. [CrossRef]
114. George, M.A.; Ramakrishna, B.L.; Glaunsinger, W.S. Electron paramagnetic resonance investigation of free radicals in polyimide films. *J. Phys. Chem.* **1990**, *94*, 5159–5164. [CrossRef]
115. Rasmussen, K.; Grampp, G.; van Eesbeek, M.; Rohr, T. Thermal and UV degradation of polymer films studied in situ with ESR spectroscopy. *ACS Appl. Math. Int.* **2012**, *2*, 1879–1883. [CrossRef]

116. Wu, J.; Miyahara, A.; Khan, A.R.; Iwata, M.; Toyoda, K.; Cho, M.; Zheng, X.Q. Effects of ultraviolet irradiation and atomic oxygen erosion on total electron emission yield of polyimide. *IEEE Trans. Plasma Sci.* **2014**, *42*, 191–198. [CrossRef]
117. Bungay, C.; Tiwald, T.E.; Devries, M.J.; Dworak, B.J.; Woollam, J.A. Characterization of UV irradiated space application polymers by spectroscopic ellipsometry. *Polym. Eng. Sci.* **2000**, *40*, 300–309. [CrossRef]
118. Alegaonkar, P.S.; Bhoraskar, V.N.; Balaya, P.; Goyal, P.S. Dielectric properties of 1 MeV electron-irradiated polyimide. *Appl. Phys. Lett.* **2002**, *80*, 640. [CrossRef]
119. Adamec, V. Temporary changes in electrical properties of polymer dielectrics due to ionizing radiation. *J. Polym. Sci.* **1968**, *6*, 1241–1253. [CrossRef]
120. Seidl, T.; Plotnikov, A.; Mustafin, E.; Lopez, R.; Severin, D.; Floch, E.; Trautmann, C.; Golubev, A.; Smolyakov, A.; Tommastini, D.; et al. Influence of swift ion beams and protons on the dielectric strength of polyimide. *Polym. Degr. Stab.* **2012**, *97*, 2396–2402. [CrossRef]
121. Shah, N.; Singh, N.L.; Desai, C.F.; Singh, K.P. Microhardness and radiation damage studies of proton irradiated Kapton films. *Rad. Meas.* **2003**, *36*, 699–702. [CrossRef]
122. Woollam, J.A.; Bungay, C.; Hilfiker, J.; Tiwald, T. VUV and IR spectroellipsometric studies of polymer surfaces. *Nucl. Inst. Meth. Phys. Res. B* **2003**, *208*, 35–39. [CrossRef]
123. Bolt, R.O.; Garrol, J.G. *Radiation Effects on Organic Materials*; Academic: New York, NY, USA, 1963.
124. Mathakari, N.L.; Bhoraskar, V.N.; Dhole, S.D. MeV energy electron beam induced damage in isotactic polypropylene. Nucl. Instrum. *Methods Phys. Res. B* **2008**, *266*, 3075. [CrossRef]
125. Bovey, F.A. *The Effect of Ionizing Radiation on Natural and Synthetic High Polymers*; Interscience: New York, NY, USA, 1958.
126. Rahnamoun, A.; Engelhart, D.P.; Humagain, S.; Plis, E.; Kennedy, W.J.; Koerner, H.; Cooper, R.; Greenbaum, S.G.; Hoffmann, R.; van Duin, A.C.T. Chemical dynamics characteristics of Kapton polyimide damaged by electron beam irradiation. *J. Chem. Phys.* **2019**. Submitted. [CrossRef]
127. Mathakari, N.L.; Bhoraskar, V.N.; Dhole, S.D. 6MeV pulsed electron beam induced surface and structural changes in polyimide. *Mater. Sci. Eng. B* **2010**, *168*, 122–126. [CrossRef]
128. Shen, Z.; Mu, Y.; Ding, Y.; Liu, Y.; Zhao, C. Study on the mechanical property of polyimide film in space radiation environments. In *Selected Papers of the Photoelectronic Technology Committee Conferences Held November 2015*; SPIE Press: Bellingham, DC, USA, 2016. [CrossRef]
129. Tsai, F.-Y.; Kuo, Y.-H.; Harding, D.R. Properties and structure of vapor-deposited polyimide upon electron-beam irradiation. *J. Appl. Phys.* **2006**, *99*, 64910. [CrossRef]
130. Zicai, S.; Yuming, L.; Weiquan, F.; Chunqing, Z.; Yigang, D. Degradation of mechanical properties of spacecraft polyimide film exposed to radiation environments. *Astrophys. Space Sci. Proc.* **2013**, *32*, 469–482. [CrossRef]
131. Spindel, A.; Reed, R.P.; Tupper, M.; Darr, J.; Pollock, D. Low-temperature electron irradiation of insulating films and adhesives. In *Advances in Cryogenic Engineering Materials*; Reed, R.P., Fickett, F.R., Summers, L.T., Stieg, M., Eds.; An International Cryogenic Materials Conference Publication, vol 40; Springer: Boston, MA, USA, 2018.
132. Sasuga, T.; Hayakawa, N.; Yoshida, K.; Hagiwara, M. Degradation in tensile properties of aromatic polymers by electron beam irradiation. *Polymer* **1985**, *86*, 1039–1045. [CrossRef]
133. Kang, P.-H.; Jeon, Y.-K.; Jeun, J.-P.; Shin, J.-W.; Nho, Y.-C. Effect of electron beam irradiation on polyimide film. *J. Ind. Eng. Chem.* **2008**, *14*, 672–675. [CrossRef]
134. Pei, X.; Wang, Q. Effect of Electron Radiation on the Tribological Properties of Polyimide. *Tribol. Trans.* **2007**, *50*, 268–272. [CrossRef]
135. Hill, D.J.T.; Hopewell, J.L. Effects of 3 MeV proton irradiation on the mechanical properties of polyamide films. *Radiat. Phys. Chem.* **1996**, *48*, 533–537. [CrossRef]
136. Kim, D.-W.; Kim, D.-I.; Huh, Y.-H.; Yang, T.-K.; Kim, Y.-S.; Ha, M.-G.; Won, M.-S.; Kim, K.-R.; Lee, J.-H. Influence of MeV protons on mechanical properties of ITO/aluminum-coated Kapton designed foe space missions. *Nucl. Instr. Meth. Phys. Res. B* **2008**, *266*, 3263–3274. [CrossRef]
137. Dever, J.A.; Messer, R.; Powers, C.; Townsend, J.; Wooldrifge, E. Effects of vacuum ultraviolet radiation on thin polyimide films. *High Perform. Polym.* **2001**, *13*, S391–S399. [CrossRef]
138. Russell, D.A.; Fogdall, L.B.; Bohnhoff-Hlavacek, G. *Simulated Space Environmental Testing on Thin Films*; NASA/CR-2000-210101; NASA: Washington, DC, USA, 2000.

139. Li, R.; Li, C.; He, S.; Di, M.; Yang, D. Damage effect of the keV proton irradiation on aluminized Kapton film. *Rad. Phys. Chem.* **2008**, *77*, 482–489. [CrossRef]
140. Ennis, C.P.; Kaiser, R.I. Mechanistical studies on the electron-induced degradation of polymethylmethacrylate and Kapton. *Phys. Chem. Chem. Phys.* **2010**, *12*, 14902–14915. [CrossRef]
141. Mishra, R.; Tripathy, S.P.; Sinha, D.; Dwivedi, K.K.; Shosh, S.; Khathing, D.T.; Muller, M.; Fink, D.; Chung, W.H. Optical and electrical properties of some electron and proton irradiated polymers. *Nucl. Ins. Meth. Phys. Res. B* **2000**, *168*, 59–64. [CrossRef]
142. Engelhart, D.P.; Plis, E.; Cooper, R.; Humagain, S.; Koch, A.; Brunetti, M.; Greenbaum, S.; Hoffmann, R. Effect of Electron Bombardment on Polyimide Film. *Key Eng. Mater.* **2018**, *759*, 48–53. [CrossRef]
143. Castle, J.G. *Measurements of Material Properties for Solar Cells*; NASA Report NASA-CR-150797; NASA: Washington, DC, USA, 1978. Available online: https://ntrs.nasa.gov/search.jsp?R=19780023588 (accessed on 9 January 2019).
144. Rai, V.N. Optical properties of neutron and proton irradiated Kapton foil. *Appl. Opt.* **1989**, *28*, 2450–2451. [CrossRef]
145. Ishida, H.; Wellinghoff, S.T.; Baer, E.; Koenig, J.L. Spectroscopic Studies of Poly[*N*,*N*′-bis(phenoxyphenyl)pyromellitimide]. 1. Structures of the Polyimide and Three Model Compounds. *Macromolecules* **1980**, *13*, 826–834. [CrossRef]
146. LaFemina, J.P.; Arjavalingam, G.; Hougham, G. Electronic structure and ultraviolet absorption spectrum of polyimide. *J. Chem. Phys.* **1989**, *90*, 5154–5160. [CrossRef]
147. Komiyama, Y.; Miyake, H.; Tanaka, Y.; Takada, T. *Observation of Surface Discharge Phenomena on Dielectric Films Under Low Pressure Using Pockels Effect in Protection of Materials and Structures from the Space Environment*; Kleiman, M.T.J., Kimoto, Y., Eds.; Springer: Berlin/Heidelberg, Germany, 2012; p. 456.
148. Sun, Y.M.; Zhu, Z.Y.; Jin, Y.F.; Liu, C.L.; Wang, Z.G.; Zhang, Q.X. The effects of high electronic energy loss on the chemical modification of polyimide. *Nucl. Instrum. Meth. B* **2002**, *193*, 214–220. [CrossRef]
149. Shi, J.; Gong, C.; Tian, X.; Yang, S.; Chu, P.K. Optical properties and chemical structures of Kapton-H film after proton irradiation by immersion in a hydrogen plasma. *Appl. Surf. Sci.* **2012**, *258*, 3829–3834. [CrossRef]
150. Alegaonkar, P.S.; Bhoraskar, V.N. Characterization of polyimide irradiated in silver solution with a pulsed electron beam. *Nucl. Insr. Meth. Phys. Res. B* **2004**, *225*, 267–274. [CrossRef]
151. Mishra, R.; Triphany, S.P.; Dwivedi, K.K.; Khathing, D.T.; Ghosh, S.; Muller, M.; Fink, D. Modification in etching characteristics and surface topography of some electron irradiated polymers. *Radiat. Meas.* **2001**, *34*, 95–98. [CrossRef]
152. Coulter, D.R.; Gupta, A.; Smith, M.V. *The Effects of Energetic Proton Bombardment on Polymeric Materials: Experimental Studies and Degradation Models*; NASA Report 19860018724; NASA: Washington, DC, USA, 1986. Available online: https://ntrs.nasa.gov/search.jsp?R=19860018724 (accessed on 8 September 2018).
153. Himmelbauer, M.; Arenholz, E.; Bäuerle, D.; Schilcher, K. UV-laser-induced surface topology changes in polyimide. *Appl. Phys. A* **1996**, *63*, 337–339. [CrossRef]
154. Mishra, R.; Tripathy, S.P.; Dwivedi, K.K.; Khathing, D.T.; Ghosh, S.; Muller, M.; Fink, D. Spectroscopic and thermal studies of electron irradiated polyimide. *Radiat. Meas.* **2003**, *36*, 621–624. [CrossRef]
155. Mishra, R.; Tripathy, S.P.; Dwivedi, K.K.; Khathing, D.T.; Ghosh, S.; Fink, D. Dose-dependent modification in makrofol-N and polyimide by proton irradiation. *Rad. Meas.* **2003**, *36*, 719–722. [CrossRef]
156. Alegaonkar, P.S.; Bhoraskar, V.N. Effect of MeV electron irradiation on the free volume of polyimide. *Radiat. Eff. Defects Solids* **2004**, *159*, 511–516. [CrossRef]
157. Hirade, T.; Oka, T.; Morishita, N.; Idesaki, A.; Shimada, A. Positron annihilation lifetime of irradiated polyimide. *Mater. Sci. Forum.* **2013**, *733*, 151–154. [CrossRef]
158. Mahapatra, S.K.; Dhole, D.D.; Bhoraskar, V.N. Growth and decay of surface voltage on silver diffused polyimide exposed to 3–15 keV electrons. *J. Phys. D Appl. Phys.* **2007**, *40*, 1097–1102. [CrossRef]
159. Mahapatra, S.K.; Dhole, S.D.; Bhoraskar, V.N. Dependence of charge buildup in the polyimide on the incident electron energy. *J. Appl. Phys.* **2006**, *100*, 34913. [CrossRef]
160. Clough, R.L. High-energy radiation and polymers: A review of commercial processes and emerging applications. *Nucl. Inst. Meth. Phys. Res. B* **2001**, *185*, 8–33. [CrossRef]
161. Sharma, V.K.; Mahajan, J.; Bhattacharyyalia, P.K. Electron beam (Eb) crosslinking of PVC insulation in presence of sensitiser additives. *Rad. Phys. Chem.* **1995**, *45*, 695–701. [CrossRef]

162. Zimek, Z.; Przybytniak, G.; Nowicki, A. Optimization of electron beam crosslinking of wire and cable insulation. *Radiat. Phys. Chem.* **2012**, *81*, 1398–1403. [CrossRef]
163. Dadbin, S.; Frounchi, M.; Saeid, M.H.; Gangi, F. Molecular structure and physical properties of E-beam crosslinked low-density polyethylene for wire and cable insulation applications. *J. Appl. Polym. Sci.* **2002**, *86*, 1959–1969. [CrossRef]
164. Ramachandran, P.; Naskar, K.; Nando, G.B. Exploring the effect of radiation crosslinking on the physico-mechanical, dynamic mechanical and dielectric properties of EOC–PDMS blends for cable insulation applications. *Polym. Adv. Tech.* **2017**, *28*, 80–93. [CrossRef]
165. Min, J.; Tao, Z.; Song, X.; Zhang, J.; Wang, Z.; Ji, Y.; Zhai, G.; Ye, X. Study on electron beam cross-linked ethylene-tetrafluoroethylene copolymer-insulated cables for aerospace applications: Mechanical performance, crystallization kinetics, and fluoride precipitation. *Polym. Adv. Tech.* **2018**, *29*, 1497–1506. [CrossRef]
166. Cleland, M.R.; Parks, L.A.; Cheng, S. Applications for radiation processing of materials. *Nucl. Inst. Meth. Phys. Res. B* **2003**, *208*, 66–73. [CrossRef]
167. Mishra, J.K.; Chang, Y.W.; Lee, B.C.; Ryu, S.H. Mechanical properties and heat shrinkability of electron beam crosslinked polyethylene–octene copolymer. *Rad. Phys. Chem.* **2008**, *77*, 675–679. [CrossRef]
168. Yang, S.L.; Wu, Z.H.; Yang, W.; Yang, M.B. Thermal and mechanical properties of chemical crosslinked polylactide (PLA). *Polym. Test.* **2008**, *27*, 957–963. [CrossRef]
169. Berg, G.J.; McBride, M.K.; Wang, C.; Bowman, C.N. New directions in the chemistry of shape memory polymers. *Polymer* **2014**, *55*, 5849–5872. [CrossRef]
170. Chernous, D.A.; Shil'ko, S.V.; Pleskachevskii, Y.M. Description of the Shape Memory Effect of Radiation-Modified Polymers under Thermomechanical Action. *J. Eng. Phys. Thermophys.* **2004**, *77*, 6–10. [CrossRef]
171. Hearon, K.; Nash, L.D.; Volk, B.L.; Ware, T.; Lewicki, J.P.; Voit, W.E.; Wilson, T.S.; Maitland, D.J. Electron beam crosslinked polyurethane shape memory polymers with tunable mechanical properties. *Macromol. Chem. Phys.* **2013**, *214*, 1258–1272. [CrossRef]
172. Xie, F.; Liu, L.; Gong, X.; Huang, L.; Leng, J.; Liu, Y. Effects of accelerated aging on thermal, mechanical and shape memory properties of cyanate-based shape memory polymer: I vacuum ultraviolet radiation. *Polym. Degr. Stab.* **2017**, *138*, 91–97. [CrossRef]
173. Hou, L.; Wu, Y.; Guo, B.; Shan, D.; Zong, Y. Degeneration and damage mechanism of epoxy-based shape memory polymer under 1 MeV electron irradiation. *Mater. Lett.* **2018**, *222*, 37–40. [CrossRef]
174. Gao, H.; Lan, X.; Liu, L.; Xiao, X.; Liu, Y.; Leng, J. Study on performances of colorless and transparent shape memory polyimide film in space thermal cycling, atomic oxygen and ultraviolet irradiation environments. *Smart. Mater. Struct.* **2017**, *26*, 095001. [CrossRef]
175. Oshima, A.; Shiraki, F.; Fujita, H.; Washio, M. Surface modification of polymeric materials using ultra low energy electron beam irradiation. *Rad. Phys. Chem.* **2011**, *80*, 196–200. [CrossRef]
176. Srinivasan, R.; Braren, B. Ultraviolet laser ablation of organic polymers. *Chem. Rev.* **1989**, *89*, 1303–1316. [CrossRef]
177. Hiraoka, H.; Lazare, S. Surface modifications of Kapton and cured polyimide films by ArF excimer laser: Applications to imagewise wetting and metallization. *Appl. Surf. Sci.* **1990**, *46*, 264–271. [CrossRef]
178. Adhi, K.P.; Owings, R.L.; Railkar, T.A.; Brown, W.D.; Malshe, A.P. Chemical modifications in femtosecond ultraviolet (248 nm) excimer laser radiation-processed polyimide. *Appl. Surf. Sci.* **2004**, *225*, 324–331. [CrossRef]
179. Du, Q.; Liu, J.; Guo, L.; Lv, M.; Zeng, X. Tailoring the surface wettability of polyimide by UV laser direct texturing in different gas atmospheres. *Mater. Des.* **2016**, *104*, 134–140. [CrossRef]
180. Du, Q.; Chen, T.; Liu, J.; Zeng, X. Surface microstructure and chemistry of polyimide by single pulse ablation of picosecond laser. *Appl. Surf. Sci.* **2018**, *434*, 588–595. [CrossRef]
181. Lorenz, P.; Lorenz, P.; Bayer, L.; Bayer, L.; Ehrhardt, M.; Ehrhardt, M.; Zimmer, K.; Zimmer, K.; Engisch, L. Nanosecond laser-induced ablation and laser-induced shockwave structuring of polymer foils down to sub-µm patterns. *Proc. SPIE* **2015**, *9351*, 935119. [CrossRef]
182. Reddy, M.R.; Srinivasamurthy, N.; Agrawal, B.L. Atomic oxygen protective coatings for Kapton film: A review. *Surf. Coat. Tech.* **1993**, *58*, 1. [CrossRef]
183. Schuler, P.; Mojazza, H.B.; Haghighat, R. Atomic oxygen resistant films for multi-layer insulation. *High Perform. Polym.* **2000**, *12*, 113. [CrossRef]

184. Devapal, D.; Packirisamy, S.; Korulla, R.M.; Ninan, K.N. Atomic oxygen resistant coating from poly (tetramethyldisilylene-co-styrene). *J. Appl. Polym. Sci.* **2004**, *94*, 2368. [CrossRef]
185. Duo, S.; Li, M.; Zhu, M.; Zhou, Y. Polydimethylsiloxane/silica hybrid coatings protecting Kapton from atomic oxygen attack. *Mater. Chem. Phys.* **2008**, *112*, 1093. [CrossRef]
186. Zhang, X.; Wu, Y.; Liu, G.; He, S.; Yang, D. Investigation on sol–gel boehmite-AlOOH films on Kapton and their erosion resistance to atomic oxygen. *Thin Solid Film.* **2008**, *516*, 5020. [CrossRef]
187. Hu, L.; Li, M.; Xu, C.; Luo, Y. Perhydropolysilazane derived silica coating protecting Kapton from atomic oxygen attack. *Thin Solid Film.* **2011**, *520*, 1063. [CrossRef]
188. Qi, H.; Qian, Y.; Xu, J.; Li, M. Studies on atomic oxygen erosion resistance of deposited Mg-alloy coating on Kapton. *Corros. Sci.* **2017**, *124*, 56. [CrossRef]
189. Wang, X.; Li, Y.; Qian, Y.; Qi, H.; Li, J.; Sun, J. Mechanically Robust Atomic Oxygen-Resistant Coatings Capable of Autonomously Healing Damage in Low Earth Orbit Space Environment. *Adv. Mater.* **2018**, *30*, 1803854. [CrossRef] [PubMed]
190. Qi, H.; Qian, Y.; Xu, J.; Zuo, J.; Li, M. An AZ31 magnesium alloy coating for protecting polyimide from Erosion-Corrosion by Atomic Oxygen. *Corros. Sci.* **2018**, *138*, 170. [CrossRef]
191. Sibin, K.P.; Esther, A.C.; Shashikala, H.D.; Dey, A.; Sridhara, N.; Sharma, A.K.; Barshilia, H.C. Environmental stability of transparent and conducting ITO thin films coated on flexible FEP and Kapton® substrates for spacecraft applications. *Sol. Energy Mater. Sol. Cell.* **2018**, *176*, 134. [CrossRef]
192. Connell, J.W.; Smith, J.G., Jr.; Hergenrother, P.M. The effect of oxygen plasma on some experimental polymers containing silicon and phosphorus. *J. Fire Sci.* **1993**, *11*, 137. [CrossRef]
193. Connell, J.W. The effect of low earth orbit atomic oxygen exposure on phenylphosphine oxide-containing polymers. *High Perform. Polym.* **2000**, *12*, 43. [CrossRef]
194. Devapal, D.; Packirisamy, S.; Nair, C.R.; Ninan, K.N. Phosphazene-based polymers as atomic oxygen resistant materials. *J. Mater. Sci.* **2006**, *41*, 5764. [CrossRef]
195. Liu, B.; Ji, M.; Liu, J.; Fan, L.; Yang, S. Phenylphosphine oxide containing polyimide matrix resins for atomic oxygen-resistant fiber-reinforced composites. *High Perform. Polym.* **2013**, *25*, 907. [CrossRef]
196. Xiao, F.; Wang, K.; Zhan, M.S. Atomic oxygen resistant phosphorus-containing polyimides for LEO environment. *J. Mater. Sci.* **2012**, *47*, 4904. [CrossRef]
197. Su, L.; Tao, L.; Wang, T.; Wang, Q. Phenylphosphine oxide-containing aromatic polyamide films with high atomic oxygen erosion resistance. *Polym. Degrad. Stab.* **2012**, *97*, 981. [CrossRef]
198. Song, G.; Li, X.; Jiang, Q.; Mu, J.; Jiang, Z. A novel structural polyimide material with synergistic phosphorus and POSS for atomic oxygen resistance. *RSC Adv.* **2015**, *5*, 11980. [CrossRef]
199. Wei, J.H.; Gang, Z.X.; Ming, L.Q.; Wei, Z.H.; Dong, D.G.; Hai, C.C. Atomic oxygen resistant phosphorus-containing copolyimides derived from bis [4-(3-aminophenoxy) phenyl] phenylphosphine oxide. *Polym. Sci. Ser. B.* **2014**, *56*, 788. [CrossRef]
200. Chunbo, W.; Haifu, J.; Dongbo, T.; Wei, Q.; Chunhai, C.; Xiaogang, Z.; Hongwei, Z.; Daming, W. Atomic oxygen effects on polymers containing silicon or phosphorus: Mass loss, erosion yield, and surface morphology. *High Perform. Polym.* **2018**. [CrossRef]
201. Zhao, Y.; Gao, H.; Li, G.M.; Liu, F.F.; Dai, X.M.; Dong, Z.X.; Qiu, X.P. Synthesis and AO Resistant Properties of Novel Polyimide Fibers Containing Phenylphosphine Oxide Groups in Main Chain. *Chin. J. Polym. Sci.* **2019**, *37*, 59. [CrossRef]